Volume 27
DOE/DP40200-25

LLE Review

Quarterly Report

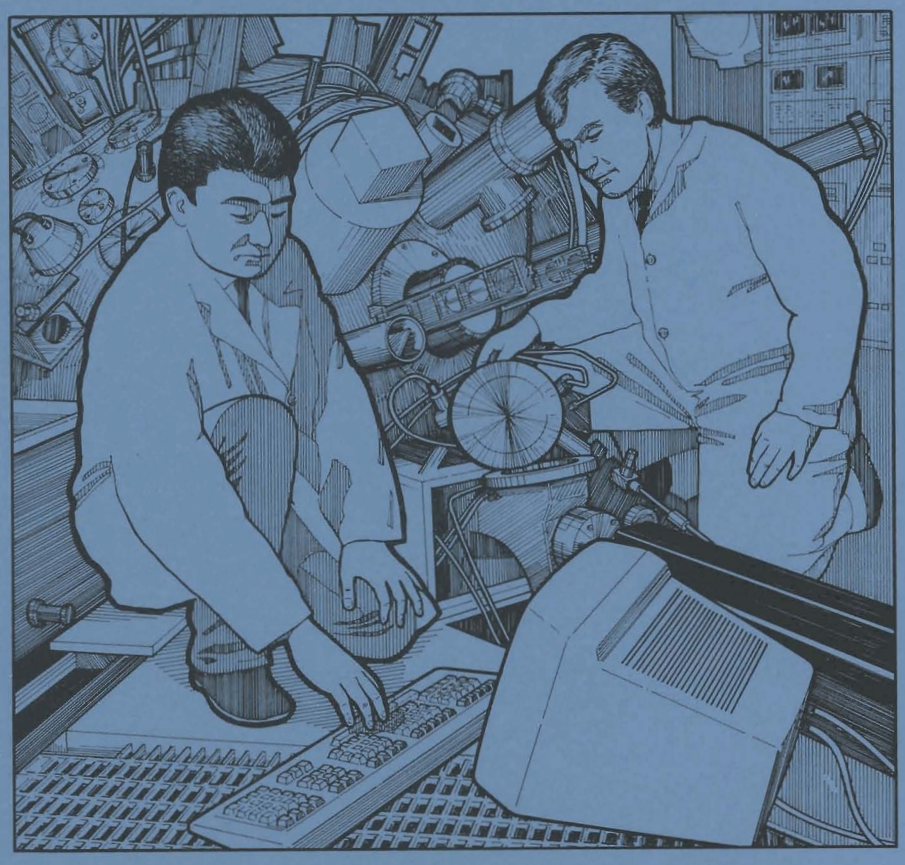

April–June 1986

Laboratory for Laser Energetics
College of Engineering and Applied Science
University of Rochester
250 East River Road
Rochester, New York 14623-1299

Volume 27
DOE/DP40200-25

LLE Review

Quarterly Report

Editor: B. Yaakobi
(716) 275-4926

April–June 1986

Laboratory for Laser Energetics
College of Engineering and Applied Science
University of Rochester
250 East River Road
Rochester, New York 14623-1299

IN BRIEF

This volume of the LLE Review, covering the period April–June 1986, contains reports on GDL and OMEGA laser activities; analysis of neutron diagnostic methods of compressed laser targets; modeling of nonlocal heat flow in laser-heated plasmas; and developments in advanced technology areas at LLE: protective polymeric coatings for nonlinear optical materials, time-resolved observation of electron-phonon relaxation in copper, and noncontact electro-optic sampling of high-speed electrical waveforms with a gallium-arsenide injection laser. Finally, the National Laser Users Facility activities for this period are summarized.

The following are highlights of the research reports contained in this issue:

- A method has been developed for measuring the ρR product of laser-compressed targets. The method involves doping the DT fuel with the isotope ^{80}Kr, which is activated by the fusion-generated neutrons via the (n, 2n) reaction to yield ^{79m}Kr whose γ decay is counted following the capture of target debris. The method is compared with those involving (a) activation of the glass shell and (b) neutron scattering of fuel ions.
- A model for treating nonlocal effects in heat transport due to long mean-free-path electrons was developed and compared to hydrodynamic code results, which do not include these effects. Nonlocal effects were found to be insignificant in the heat transport of laser-generated plasmas.

- An organosilicone resin was found to be useful for the deposition of laser-damage-resistant, antireflectance or protective coatings on KDP, lithium niobate, and potassium pentaborate. The availability of multilayer dielectric thin-film coatings on these nonlinear optical materials, using high laser-damage resistance and good mechanical and environmental durability will be very useful in the harmonic conversion of high-power lasers where now complex geometries, involving index-matching fluids, have to be used.
- Electron-phonon relaxation time in copper has been directly measured by monitoring the laser-heating-induced modulation of the transmissivity of thin copper films. Nonequilibrium heating with a large difference between electron and lattice temperatures has been demonstrated.
- The ability to make noncontact measurements of electrical waveforms with 30-ps diode-laser pulses has been demonstrated. This electro-optic sampling method utilizes a substrate-independent probe and is inexpensive and practical.

CONTENTS

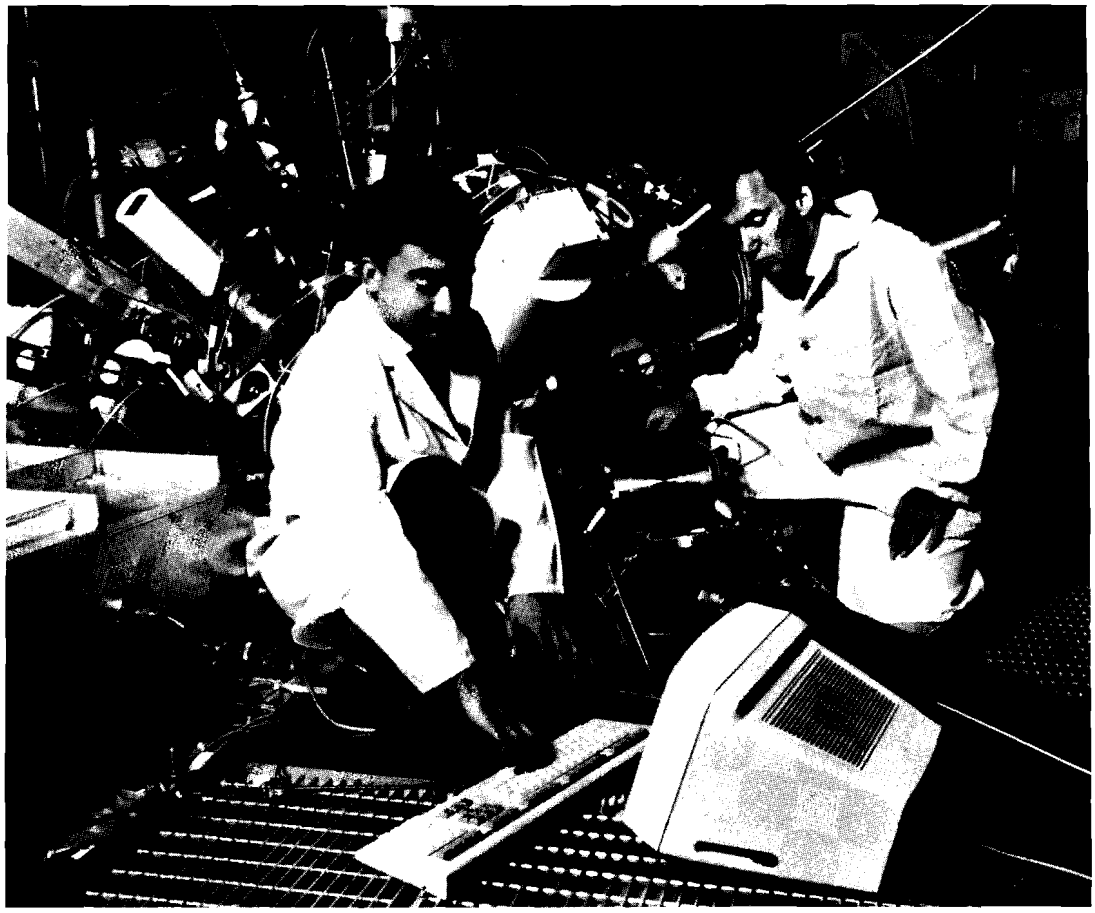

Lead experimental engineer Gregory Pien (left) and OMEGA experimental group leader Martin Richardson (right) survey the computer-controlled, rapid-retraction system for nuclear activation analysis of target debris.

Section 1
LASER SYSTEM REPORT

1.A GDL Facility Report

The glass development laser (GDL) facility has returned to service as a target interaction facility during this quarter. By mid-April, the system had been modified to include a free-propagation path for the oscillator output, and was realigned. Throughout May and June, the system was used in target experiments. Maximum beam energy achieved was 685 J (at 1054 nm). This energy was reached with the active-mirror output amplifiers configured for double pass amplification.

A summary of GDL operations follows:

System Alignment and Pointing Shots	165
Calibration and Characterization Shots	55
Target Shots and Focus Scans	160
TOTAL	380

1.B OMEGA Facility Report

During the third quarter of FY86 OMEGA continued full operation as a 351-nm target irradiation facility. The emphasis was on satisfying experimental requirements for various target interaction studies, assessment of the state of uniformity of the OMEGA beams, and engineering of the driver-line free-propagation upgrade, scheduled for implementation this summer.

Throughout the quarter, target experiments consumed at least two days of every week. While the primary aim of the quarter was the study of high-density target implosions, various experimental campaigns were satisfied. Numerous shots were taken as part of the National Laser User Facility (NLUF) program, for users from the University of Maryland and the Naval Research Laboratory. Using activated krypton targets a collaborative study was conducted sampling areal densities of shells with the nuclear activation apparatus from Lawrence Livermore National Laboratory (LLNL). Other target interaction studies included coronal physics, time-resolved ionization studies, diagnostic development, on-target uniformity, absorption, and beamline/on-target streak camera correlation.

In addition to conducting laser-target interaction experiments, the laser system was used in carrying out various beam uniformity programs.

A summary of the operation of OMEGA follows:

Driver Alignment and Test Shots	76
Beamline Test and Calibration Shots	192
Target Shots	188
TOTAL	456

ACKNOWLEDGMENT

This work was supported by the U.S. Department of Energy Office of Inertial Fusion under agreement No. DE-FC08-85DP40200 and by the Laser Fusion Feasibility Project at the Laboratory for Laser Energetics, which has the following sponsors: Empire State Electric Energy Research Corporation, General Electric Company, New York State Energy Research and Development Authority, Ontario Hydro, Southern California Edison Company, and the University of Rochester. Such support does not imply endorsement of the content by any of the above parties.

Section 2
PROGRESS IN LASER FUSION

2.A Neutron Diagnosis of Compressed ICF Targets

With the development of large, short-wavelength laser systems, such as the 24-beam OMEGA laser,[1] high-yield and high-density laser-fusion experiments can be undertaken. Since the first kilojoule, short-wavelength laser experiments at the beginning of 1985,[2] the highest measured neutron yield has gone up by over a factor of 300, in experiments performed by three laboratories.[3-5] In the most recent experiment,[5] a neutron yield of 1.1×10^{13} was achieved. This corresponds to a yield efficiency (thermonuclear energy divided by the laser energy) of 1.5×10^{-3}. The generation of high fluences of neutrons in ICF experiments permits the development of neutron-dependent diagnostic approaches to the determination of compressed core parameters. We review here a number of these diagnostics, some of which have been deployed on OMEGA for assessing the implosion uniformity. In particular, we stress that simultaneous measurements of several parameters of the compressed core at the time of neutron generation are necessary for unambiguous evaluation of the symmetry and integrity of the thermonuclear burn region.

The compressed core parameters accessible through neutron-dependent diagnostics, at present activated on the OMEGA facility or under development, are listed in Table 27.I, together with estimates of their current sensitivity and resolution. In the following we review the characteristics and limitations of these diagnostics.

Neutron fluence from a transient point source can be measured by a variety of techniques with high accuracy ($<1\%$) for neutron yields

Table 27.I
Neutron diagnostics of compressed fusion targets.

Target Parameter	Diagnostic Approach	Sensitivity, Resolution
Neutron fluence (Y_n)	scintillator/photomultipliers	$Y_n > 10^4$, $\Delta\Omega \sim 10^{-3}$ sr
	Ag (n, β^-) Cd	$Y_n > 10^6$, $\Delta\Omega \sim 10^{-2}$ sr
	^{63}Cu(n, 2n) ^{62}Cu	$Y_n > 10^6$, $\Delta\Omega \sim 10^{-2}$ sr
	^{208}Pb(n, 2n) ^{207m}Pb	$Y_n > 10^6$, $\Delta\Omega \sim 10^{-2}$ sr
Neutron energy spectrum [n(E) dE]	neutron TOF spectrometry	$Y_n > 10^8$, $\Delta\Omega \sim 10^{-4}$ sr, $\Delta E \sim 1$ KeV
Neutron emission time [n(t)]	neutron streak camera	$Y_n > 10^{10}$, $\Delta\Omega \sim 10^{-2}$ sr, $\Delta t \gtrsim 10$ ps
Neutron emission region [n(R)]	pinhole imaging	
	zone-plate-coded imaging	$Y_n > 10^{12}$, $\Delta R \sim 5\,\mu$m
	penumbral imaging	$Y_n > 10^{11}$, $\Delta R \sim 10\,\mu$m
	zone-plate-coded imaging (α particles)	$Y_n > 10^8$, $\Delta R \sim 5\,\mu$m
Fuel $<\rho R>$	knock-on DT ion spectrometry	$(Y_n \cdot <\rho R>) > 10^6$ g/cm^2, $\Delta\Omega \sim 10^{-2}$ sr
	^{80}Kr (n,2n) ^{79m}Kr activation	$(Y_n \cdot <\rho R>) > 10^{10}$ g/cm^2, $\Delta\Omega \sim 10^{-2}$ sr*
Shell $<\rho\Delta R>$	^{28}Si(n, p) ^{28}Al	$(Y_n \cdot <\rho\Delta R>) > 10^7$ g/cm^2, $\Delta\Omega \sim 10^{-2}$ sr

$\Delta\Omega$ = detection solid angle, ΔE = energy resolution, Δt = time resolution

*Assumes a 10^{-3} mass ratio between Kr tracer gas and DT fuel

E4058

exceeding 10^6. Most common in ICF experiments is the use of Ag-, Cu-, and Pb-activation techniques, which have high sensitivity even with counting times of less than five minutes and relatively small collection-solid-angles $\Delta\Omega$.

The ion temperature (T_i) of the fusion fuel can be measured by a variety of techniques, including neutron time-of-flight (TOF) spectrometry. For some target configurations, a simultaneous measurement of T_i through TOF spectrometry of the various fusion products is desirable. These include the deuterium-tritium (DT), 14.1-MeV neutrons and the 3.5-MeV α particles, as well as the deuterium-deuterium (DD) fusion, 3.02-MeV protons. The neutron time-of-flight spectrometer on OMEGA consists of a single ultrafast neutron detector,[6] comprising a quenched

(t_{rise} ~100 ps) scintillator, close-coupled to a GHz (t_{rise} ~500 ps) Chevron-type microchannel plate (MCP) photomultiplier, located 8.6 m from the target, in conjunction with a GHz oscilloscope.[3] In high-yield experiments without significant shielding, the MCP detector was found to be affected by γ rays produced by neutron reactions occurring in the 75-mm-thick stainless-steel target-chamber wall. This signal could be so intense as to degrade the linearity of the MCP for the neutron-burst detection. Other recording devices utilizing MCP's, such as image intensifiers in streak cameras, were similarly affected. The mean ion temperature, $<T_i>$ (keV), is deduced using Brysk's derivation[7] of the neutron energy spread, $\Delta E \approx 177 <T_i>^{1/2}$, where both ΔE and T_i are in keV. The present device has an energy resolution of ~1 keV. For future high-density experiments in which low ion temperatures ($T_i \lesssim 2$ keV) are expected, greater spectral resolution will be required.

A primary parameter of target performance is the fuel areal density $<\rho R>$ at the time of peak compression. This parameter can be determined by both x-ray and nuclear diagnostics. Although x-ray spectroscopy of tracer gases in the fuel,[8] and x-ray photography[9] of the compressed shell can provide a measure of the density of the fuel and its spatial extent, nuclear diagnostics have the advantage of diagnosing the fuel conditions at the time of neutron generation. Up to now these nuclear diagnostics have been (a) knock-on ion spectrometry,[10] providing a direct estimate of the fuel $<\rho R>$, and (b) neutron activation of Si in the shell, giving a measure of the shell areal density $<\rho \Delta R>$ and, through hydrodynamic code simulations, an estimate of the final fuel conditions. The latter technique detects the total number of ^{28}Si (n,p) ^{28}Al reactions induced in the imploding glass shell. A small known fraction of the target debris is collected in a thin Ti cone and rapidly transferred to a radiochemical counting system.[12] The number of ^{28}Si transmutations, N_s^*, is obtained by detecting the coincident 1.78-MeV γ ray and 2.86-MeV β particle decays from ^{28}Al. The shell $<\rho \Delta R>$ is then linearly related to the activation yield N_s^* by the formula[13]

$$N_s^* = f(Y_n \sigma_f A_o / A_w) \cdot <\rho \Delta R> \ , \qquad (1)$$

where σ is the cross section for the ^{28}Si (n,p) ^{28}Al reaction (0.250 b), f is the fraction of Si ions in the shell, A_o is Avogadro's number, and A_w is the average atomic weight of the shell. The value of N_s^* is determined, from the number of coincidence decays N_c detected over a time Δt starting at a time t after the laser shot, by the equation

$$N_s^* = N_c / [\eta_c \eta_d e^{-\lambda t} (1 - e^{-\lambda \Delta t})] \ , \qquad (2)$$

where η_c and η_d are the collector and detector efficiencies and λ is the ^{28}Al decay constant. The background count level of the system on OMEGA is ~ 0.54 counts/min, and thus for a signal of ten counts recorded over a five-minute interval a minimum value of the $Y_n \cdot <\rho \Delta R>$ product of $\sim 10^7$ neutron-g/cm^2 is detectable.

In the measurement of the fuel $<\rho R>$, a fraction of the deuterons and tritons scattered by 14.1-MeV neutrons in the compressed fuel is

collected by thin (140-μm) CR-39 nuclear-track detectors inserted in Ta-filtered cells, subtending a total solid angle of $\Delta\Omega \sim 1\%$. The total number of scattered fuel ions (Q) is related to the fuel conditions by[14]

$$Q = (\sigma_T <\rho_T R> + \sigma_D <\rho_D R>) Y_n , \quad (3)$$

where ρ_T and ρ_D are the triton and deuteron densities and σ_T and σ_D are their cross sections for neutron elastic scattering (0.92b and 0.62b, respectively). The number of scattered particles detected, N_t^*, is given by[14]

$$N_t^* = (0.18 / 4\pi) \Delta\Omega \epsilon <\rho R> Y_n , \quad (4)$$

where ϵ is the fraction of particles that can produce a signal in the CR-39, and is determined from its response characteristics, filter transmission functions, and other factors.[15] This simple technique provides an unambiguous measure of the fuel $<\rho R>$ for targets in which the deuteron and triton energy spectra are not moderated by passage through the compressed shell. It is ideal for the diagnosis of high-yield implosions of high-aspect-ratio targets, but is expected to be of limited value for thick-glass shell targets designed for moderately high-density (e.g., 50 × liquid density) implosions. With the fabrication of cryogenic polymer shell targets, which should provide optimal high-density performance, knock-on ion spectrometry will again become a valid $<\rho R>$ diagnostic.

An alternative approach that does not suffer from compressed-shell moderation effects depends on the activation of tracer gas elements in the fuel. The specific reaction being investigated[16] is the ^{80}Kr (n,2n) ^{79m}Kr reaction in which the ^{79m}Kr emits γ rays of energy of ~ 130 keV with a half-life of ~ 50 s. The use of krypton has the advantage that the gas is inert, does not permeate into glass, and is compatible with cryogenic targets. This technique does not have the sensitivity of knock-on ion spectrometry, but for ^{80}Kr concentrations small enough not to impair target performance ($< 10^{-3}$ Kr to DT mass ratio), it will provide a measure of $<\rho R>$ for targets having complex shell structures and high final fuel densities.

Other parameters of value in determining target performance and in comparing the latter to hydrodynamic code simulations are the time, duration, and region size of the neutron emission. Considerable effort is now being made to satisfy these demands.

Available detectors for single bursts of 14.1-MeV neutrons have temporal resolutions of ~ 400 ps,[6] insufficient to resolve the thermonuclear burn time for most fusion targets. Several approaches have been proposed or are currently under investigation to provide better than 100-ps resolution.[17-20]

Knowledge of the size of the thermonuclear burn region is important for determining the fraction of the compressed fuel region contributing to neutron generation, for assessing the local fuel conditions, and for de-

termining the symmetry of the implosion. Several approaches to imaging the neutron emission directly have been proposed, including the use of pinhole imaging, zone-plate-coded imaging,[21] and penumbral imaging.[22] All these techniques are limited in sensitivity. Nonetheless, we can expect exploratory studies in the near future with high-yield targets producing neutron yields in excess of 10^{11}. Additionally, for these targets, demonstrated techniques[23] of measuring the burn-region size by zone-plate-coded imaging of the α particles are possible. However, for targets designed to achieve high density, the α particles will be stopped in the compressed shell.

In summary, it can be seen that current fusion experiments are providing conditions that enable the development of a number of diagnostics of the compressed fuel region. It is evident that an unambiguous assessment of the physical state of the compressed fuel and of its symmetry cannot be obtained, or compared with the predictions of hydrodynamic code simulations, without the simultaneous use of several of these diagnostics.

ACKNOWLEDGMENT

This work was supported by the U.S. Department of Energy Office of Inertial Fusion under agreement Nos. DE-FC08-85DP40200 and W-7405-ENG-48, and by the Laser Fusion Feasibility Project at the Laboratory for Laser Energetics, which has the following sponsors: Empire State Electric Energy Research Corporation, General Electric Company, New York State Energy Research and Development Authority, Ontario Hydro, Southern California Edison Company, and the University of Rochester. Such support does not imply endorsement of the content by any of the above parties.

REFERENCES

1. J. M. Soures, R. J. Hutchison, S. D. Jacobs, L. D. Lund, R. L. McCrory, and M. C. Richardson, *Proceedings of the 10th Symposium on Fusion Engineering*, Philadelphia, PA, 1983 (IEEE, New York, 1984), p. 1392.

2. M. C. Richardson, W. Beich, J. Delettrez, M. Dunn, L. Folnsbee, R. J. Hutchison, S. A. Jacobs, R. Keck, T. Kessler, W. Lampeter, R. Leary, S. Letzring, F. J. Marshall, R. L. McCrory, S. Morse, R. Peck, G. Pien, C. Pruitt, D. Quick, F. Rister, W. Seka, M. Simpson, S. Skupsky, D. Smith, J. M. Soures, C. P. Verdon, W. Watson, and D. Whiteman, *Proc. Conf. on Lasers and Electro-Optics 1985*, Baltimore, MD (Optical Society of America, 1985), p. 234.

3. M. C. Richardson, P. McKenty, R. F. Keck, F. J. Marshall, D. M. Roback, C. P. Verdon, R. L. McCrory, and J. M. Soures (to be published); *Laser Interaction and Related Plasma Phenomena*, Vol. 7 (Plenum Press, NY, to be published)

4. C. Yamanaka *et al., Laser Interaction and Related Plasma Phenomena*, Vol. 7 (Plenum Press, NY, to be published).

5. S. M. Lane, M. D. Cable, S. G. Prussin, S. G. Grendinning, D. H. Munro, S. P. Hatchett, K. G. Estabrook, L. J. Suter, M. C. Richardson, P. W. McKenty, D. Roback, and C. P. Verdon, presented at 6th Topical Conf. High Temp. Plasma Diag., Hilton Head, SC (March 1986).

6. P. B. Lyons *et al.*, *Nucl. Instrum. Methods* **171**, 459 (1980).

7. H. Brysk, *Plasma Phys.* **15**, 611 (1973).

8. B. Yaakobi, D. M. Villeneuve, M. C. Richardson, J. M. Soures, R. Hutchison, and S. Letzring, *Opt. Commun.* **43**, 343 (1982).

9. M. C. Richardson, T. R. Boehly, B. A. Brinker, T. C. Bristow, R. S. Craxton, J. A. Delettrez, G. Enright, A. Entenberg, W. Friedman, L. M. Goldman, J. Hoose, R. J. Hutchison, L. Iwan, S. Kacenjar, K. Lee, S. A. Letzring, L. D. Lund, R. S. Marjoribanks, R. L. McCrory, J. M. Miller, J. Rizzo, W. D. Seka, S. Skupsky, J. M. Soures, C. P. Verdon, D. M. Villeneuve, E. A. Williams, and B. Yaakobi, in *Laser Interaction and Related Plasma Phenomena*, Vol. 6, edited by H. Hora and G. Miley, (Plenum Press, NY, 1984), p. 903.

10. S. Kacenjar, S. Skupsky, A. Entenberg, L. Goldman, and M. Richardson, *Phys. Rev. Lett.* **49**, 463 (1982).

11. E. M. Campbell, W. M. Plaeger, P. H. Lee, and S. M. Lane, *Appl. Phys. Lett.* **36**, 965 (1980).

12. E. M. Campbell, H. G. Hicks, W. C. Mead, L. W. Coleman, C. W. Hatcher, J. H. Dellis, M. J. Boyle, J. T. Larsen, and S. M. Lane, *J. Appl. Phys.* **51**, 6065 (1980).

13. S. M. Lane, E. M. Campbell, and C. Bennett, *Appl. Phys. Lett.* **37**, 600 (1980).

14. S. Skupsky and S. Kacenjar, *J. Appl. Phys.* **52**, 2608 (1981).

15. S. Kacenjar, L. M. Goldman, A. Entenberg, and S. Skupsky, *J. Appl. Phys.* **56**, 2027 (1984).

16. S. Prussin, S. M. Lane, M. C. Richardson, and S. Noyes, presented at the 6th Topical Conf. High Temp. Plasma Diagnostics, Hilton Head, SC (March 1986).

17. C. L. Wang, R. Kalibjian, and M. S. Singh, *International Congress on High-Speed Photography and Photonics* (SPIE, Bellingham, WA, 1983), Vol. 348, p. 276.

18. C. L. Wang, R. A. Lerche, H. Medicki, G. E. Phillips, and M. S. Singh, presented at the 6th Topical Conf. High Temp. Plasma Diagnostics, Hilton Head, SC (March 1986); *Rev. Sci. Instrum.* **57**, 1749 (1986).

19. H. Kislev and G. Miley, *ibid.*, 1746 (1986).

20. H. Niki *et al.*, *ibid.*, 1743 (1986).

21. R. A. Lerche, S. M. Lane, A. M. Hawryluk, and N. M. Ceglio, presented at the 6th Topical Conf. High Temp. Plasma Diagnostics, Hilton Head, SC (March 1986).

22. K. A. Nugent, B. Luther-Davies, and A. Perry, in *Laser Interaction and Related Plasma Phenomena*, Vol. 7, edited by G. Miley and H. Hora (Plenum Press, NY).

23. N. M. Ceglio and L. W. Coleman, *Phys. Rev. Lett.* **39**, 20 (1977).

2.B Modeling Nonlocal Heat Flow in Laser-Produced Plasmas

Introduction

Computer simulations of heat transport in laser-fusion experiments have generally required an upper bound to be placed on the classical heat flux[1] ($q_c = -\kappa \nabla T$) to obtain agreement with experimental results. Deviations from classical heat flow are to be expected in laser-produced plasmas because temperature scale lengths can be shorter than the mean free paths of high-velocity electrons carrying a significant fraction of the heat. Fokker-Planck calculations[2,3] of electron transport at simplified laser-fusion conditions show nonlocal effects as the electrons of long mean free path produce a non-Maxwellian isotropic distribution function, and consequently a breakdown in the classical approximations. Because of computer limitations, it has not yet been possible to include a Fokker-Planck model for thermal electrons into a laser-fusion hydrodynamics code. An approximate scheme for including nonlocal effects has been proposed by Luciani and Mora.[4] We have examined their "delocalization" model under a variety of conditions relevant to laser-driven fusion and compared the results with Fokker-Planck simulations and with the method of flux limitation.

The expression for a nonlocal heat flux obtained by Luciani and Mora is written in Eq. (1) for the case of a constant electron density and boundaries at infinity,

$$q_H(x) = \int_{-\infty}^{\infty} q_c(x') \exp\left(-|x - x'| / \lambda_H\right) dx' / 2\lambda_H , \qquad (1)$$

where

$$\lambda_H = 32 (Z + 1)^{1/2} \lambda_{ei} \text{ and } \lambda_{ei} = T^2 / [\, 4\pi n_e (Z + 1) e^4 \ln \Lambda \,] .$$

The physical significance of Eq. (1) is that the heat flux at position x is determined by the classical fluxes from other points x′ up to a distance about λ_H away. The delocalization parameter λ_H is an effective mean free path that was determined by comparison with Fokker-Planck calculations. Its magnitude corresponds to $(\lambda_{ei}\, \lambda_{ee})^{1/2}$, evaluated at the velocity 2.4 $(kT/m)^{1/2}$ that is characteristic of the electron velocities dominating the heat flow. When the density is nonuniform, λ_H is modified according to

$$\frac{|x - x'|}{\lambda_H(x')} = \int_x^{x'} \frac{n(x'')\, dx''}{n(x')\, \lambda_H(x'')} . \qquad (2)$$

More recently, Luciani and Mora[5] have added to q_H an additional term q_L accounting for inverse-Bremsstrahlung laser deposition. This

contribution has the same form as Eq. (1) with the exponent replaced by a tabulated function $A_2 [| x - x' | / \lambda_L (x')]$. This function is characterized by another delocalization parameter λ_L, which is about five times smaller than λ_H, reflecting the shorter mean free path of the low-energy electrons dominating laser absorption. The total nonlocal flux is $q_H + q_L$.

Calculating the time evolution of the temperature T from Eq. (1), we define an effective coefficient of conductivity κ^* such that

$$\bar{q} \equiv -\kappa^* \nabla T \ . \tag{3}$$

All nonlocal effects are included in κ^*. The heat-flow equation now has the classical form:

$$\frac{3}{2} nk \, dT/dt - \nabla \cdot \kappa^* \nabla T = 0 \ , \tag{4}$$

and is solved fully implicitly except at the occasional points where $\kappa^* < 0$ or where the variation of temperature across two adjacent computational cells is less than 10^{-3} T, in which case the numerical treatment is explicit. At boundaries, we impose the constraint of zero heat flux, using the reflecting condition in Ref. 4.

The degree to which nonlocal effects are important for heat transport is examined using a local flux-limited model in which an upper bound is placed on q_c in terms of the free-streaming flux

$$q_f = f \, nkT \, (kT/m)^{1/2} \ , \tag{5}$$

with an adjustable parameter f (flux limiter). Flux limitation is generally effected by either a sharp cutoff,

$$q = \min (q_c, q_f) \ , \tag{6}$$

or with an harmonic average,

$$q = (1/q_c + 1/q_f)^{-1} \ . \tag{7}$$

The latter expression is used here. Both produce similar results, but with different flux limiters. Values for f between 0.03 and 0.1 lead to agreement with experimental data.[6-8]

Because Fokker-Planck calculations are highly time consuming, comparisons between the delocalization model, flux-limited transport, and Fokker-Planck calculations were made without hydrodynamics, using a stationary plasma-density profile characteristic of laser-irradiated plasmas. The delocalization model has been implemented into the one-dimensional hydrodynamics code *LILAC*, developed at the University of

Rochester.[9] In the following, we show results of laser-fusion simulations with hydrodynamics, comparing the delocalization model with flux-limited transport and results of transport experiments.

Stationary Plasma

Cases similar to those discussed in Ref. 2, in which laser light irradiates a stationary electron-density profile, are considered, and the temperature evolution of the electrons is calculated. Results are presented for a time of 120 ps, when the temperature profile in the corona has reached a quasi steady-state condition such that laser-energy deposition is balanced by heat transport into the high-density part of the plasma.

For accuracy, two different Fokker-Planck codes[3,10] were used; they produced similar results. The delocalization model gave best agreement with the Fokker-Planck calculations when the delocalization parameters were somewhat modified: in the remaining discussion λ_H is replaced by $0.8\ \lambda_H$ and λ_L by $2\ \lambda_L$. These modifications, which affected the results by no more than 10%, brought the nonlocal results closer to those of Fokker-Planck codes in the region near the critical surface. Throughout, we use the following Coulomb logarithm[11]:

$$\ln \Lambda_{ee} = \ln \Lambda_{ei} = 24 - \tfrac{1}{2} \ln (n^{1/2}/T) \ . \qquad (8)$$

For the delocalization and flux-limited calculations, the kinetic correction to laser absorption suggested by Langdon[12] is used. Equilibration with ions is neglected in Fokker-Planck simulations.

Results are presented for irradiation with two frequencies of laser light: 1054 nm and 351 nm.

1. 1054-nm Irradiation

For 1054-nm irradiation (critical density $1 \times 10^{21}\ cm^{-3}$), the electron density profile consisted of a plateau at $10^{19}\ cm^{-3}$, which exponentially decreased with a 100-μm scale length to $5 \times 10^{19}\ cm^{-3}$ (Fig. 27.1). The laser intensity was constant at $3 \times 10^{14}\ W/cm^2$. The profile for laser-energy deposition is shown in Fig. 27.1 for a time of 120 ps.

Figure 27.2 shows the temperature profile as calculated by three different models of heat transport: (1) Fokker-Planck, (2) delocalization model, and (3) flux-limited diffusion using the harmonic means q_c and q_f. For a flux limit of 0.1 (typically used for the interpretation of experiments), we find too much heat inhibition in relation to the Fokker-Planck result. The $f = 0.2$ case more correctly models the penetration of the heat front and the temperature in the laser-deposition region. However, it cannot model nonlocal effects that lead to a reduced temperature in the low-density region and a small "foot"—produced by penetration of high-velocity electrons from hotter parts of the plasma—in the high-density region. The Fokker-Planck result has a low coronal temperature due to leakage into the high-density region of high-velocity electrons of long mean free path at a rate faster than they can be replaced by electron-electron collisions.

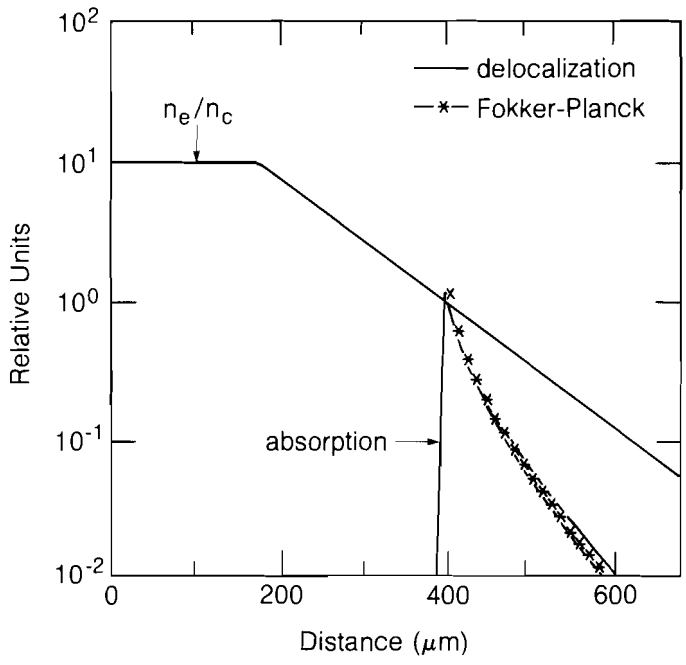

Fig. 27.1
Stationary electron density profile (relative to critical density 1×10^{21} cm^{-3}) and energy deposition profile (relative units); 1054-nm irradiation at 3×10^{14} W/cm^2, time: 120 ps.

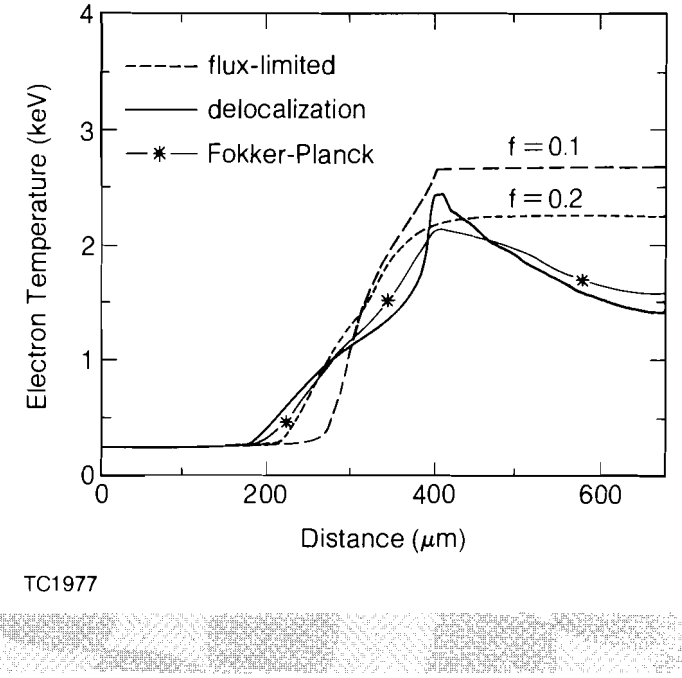

Fig. 27.2
Temperature profiles for three transport models: Fokker-Planck, delocalization, and flux-limited diffusion. The results are based on the stationary density profile of Fig. 27.1 (1054 nm, 120 ps).

Both of these nonlocal effects are qualitatively obtained with the delocalization model. Near the critical density, however, the temperature profile is too steep. The steepening can be reduced by increasing the delocalization parameter (λ_L) for absorption, but this simultaneously produces too large a foot on the heat front. Perhaps some modification is required in the tabulated attenuation function A_2, used for q_L.[3]

Similar results are obtained when the models are compared at different times during the irradiation (20 ps to 120 ps), at laser intensities of 10^{14} and 10^{15} W/cm^2, and with different ionic charges (Z = 4 and Z = 10). A summary in Table 27.II compares results for (1) penetration of the heat front (characterized by the distance between the position of the critical density n_c and the point where the temperature drops to 500 eV), (2) temperature at n_c, (3) temperature at $n = 5 \times 10^{19}$ cm^{-3}, and (4) laser-absorption fraction. The large difference (~25%) in the penetration of the 500-eV point, between local and nonlocal models, results from artificially placing an upper limit of 10^{22} cm^{-3} on the electron density. In more realistic simulations the foot of the heat front is at a density at least ten times higher, reducing the mean free path by the same factor. The difference in heat penetration among the different models becomes in this case relatively small.

Table 27.II
Comparison between three transport models: Fokker-Planck (FP), delocalization (D), and flux-limited diffusion (f = 0.2), for a stationary plasma with 1054-nm irradiation.

	10^{14} W/cm^2, Z = 10			3×10^{14} W/cm^2, Z = 4			10^{15} W/cm^2, Z = 4		
	FP	D	f=0.2	FP	D	f=0.2	FP	D	f=0.2
Penetration (μm)	175	175	140	225	230	180	250	275	215
T(keV) at 10^{21} cm^{-3}	1.3	1.3	1.3	2.1	2.3	2.1	2.3	2.6	2.4
T(keV) at 5×10^{19} cm^{-3}	1.0	0.8	1.2	1.4	1.3	2.2	1.8	1.8	2.4
Absorption	48%	45%	43%	33%	35%	35%	16%	15%	14%

TC2047

2. 351-nm Laser Irradiation

We now consider the case of irradiation by 351-nm laser light with a constant intensity of 5×10^{14} W/cm^2. The electron density profile is steeper (scale length = 25 μm) than for 1054-nm irradiation, which is characteristic of short-wavelength illumination. The peak density is an order of magnitude higher, to accommodate the higher critical density (9×10^{21} cm^{-3}). Figure 27.3 shows the density profile, together with the laser energy deposition (at 120 ps) for the case Z = 4.

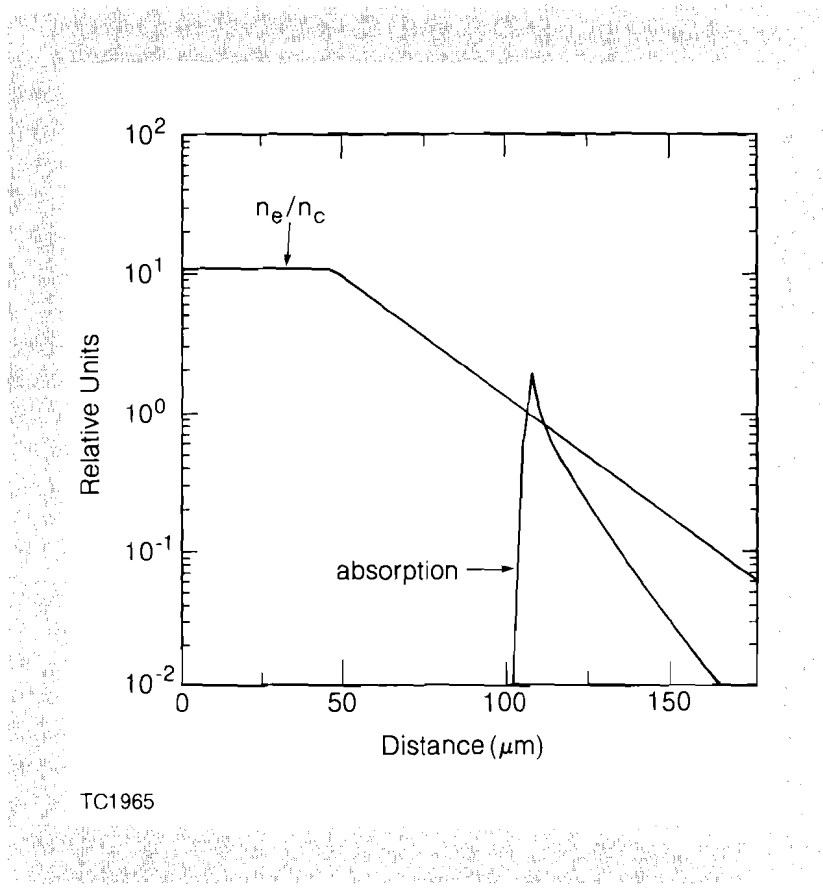

Fig. 27.3
Same as Fig. 27.1, but for 351-nm irradiation with a critical density of 9×10^{21} cm^{-3}.

The temperature profiles at 120 ps (351-nm irradiation) are compared in Fig. 27.4 for the three models. The flux-limited result (f = 0.1) shows much better agreement with the Fokker-Planck calculation than was the case for 1054-nm irradiation, because nonlocal effects are now less important. A flux limiter of 0.2 produces similar results. The smaller density scale length here is more than compensated for by the smaller mean free path produced by higher density and lower temperature. However, the delocalization model shows much worse agreement with Fokker-Planck calculations in the underdense region. Apparently, there is too much heat leakage from the corona to the high-density region. This can be improved by limiting the delocalization parameter λ_H so that it does not exceed about $3 \times \lambda_H (n_c)$. ($\lambda_H = 90$ μm at n_c, and it reaches a maximum of 400 μm at the lowest density considered here: 5×10^{20} cm^{-3}.) Limiting λ_H has only a small effect on the 1054-nm examples discussed earlier. Discrepancies in the low-density corona do not seriously affect heat transport into the high-density plasma.

Hydrodynamic Simulations

The delocalized heat-transport model was incorporated into the hydrocode *LILAC*,[9] to simulate laser-irradiation experiments. Minor modifications were made to account for spherical geometry; spherical effects are negligible in these calculations, however. Heat-transport experiments were simulated for both 1054-nm[6] and 351-nm[7] laser irradiations.

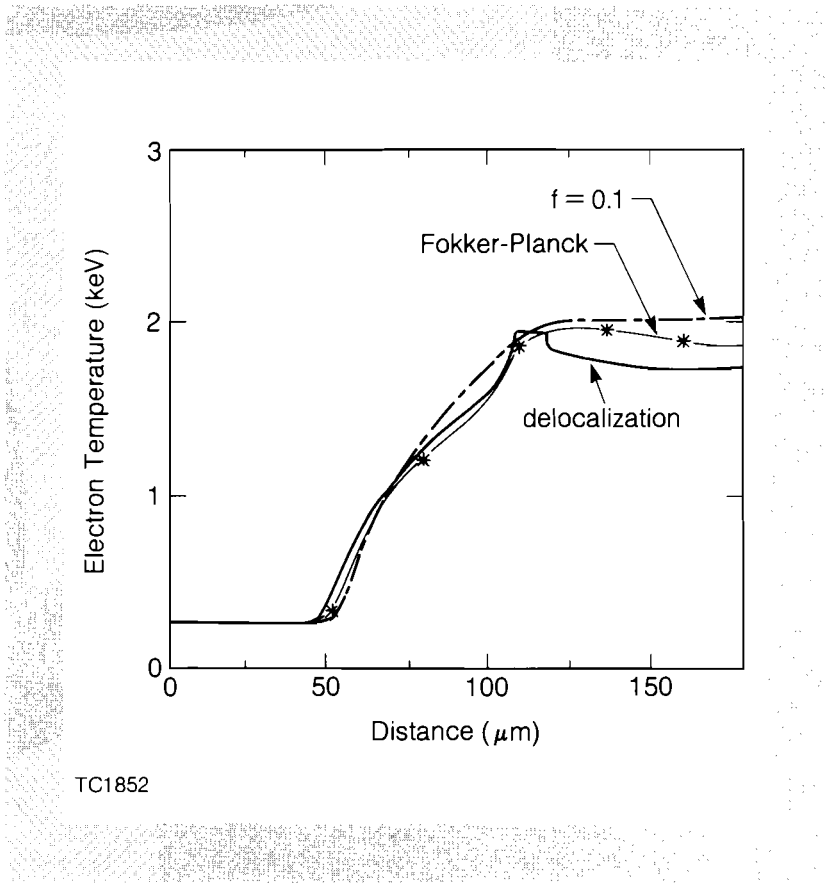

Fig. 27.4
Same as Fig. 27.2, but for 351-nm irradiation at 5×10^{14} W/cm^2, using the electron density profile of Fig. 27.3.

1. 1054-nm Irradiation

For the 1054-nm case, the laser was a 1.1-ns FWHM Gaussian pulse with a peak intensity of 3.3×10^{14} W/cm^2. The target consisted of a 186-μm-radius glass microballoon with a signature layer of either Al or Ti, which was overcoated with various thicknesses of CH. Laser refraction was treated by a geometrical ray-tracing algorithm. Absorption was calculated using Langdon's correction for kinetic effects in inverse bremsstrahlung[12] and Ref. 13 was used for describing the creation of suprathermal electrons by resonance absorption. The amount of energy deposited into suprathermal electrons was relatively small, ~20% of the absorbed energy, and these electrons were transported using *LILAC* subroutines. Equation (1) for delocalized transport was used only for the thermal component.

The calculated, maximum penetration depths into the CH layer for the 200-eV, 500-eV, and 1000-eV isotherms are listed in Table 27.III and compared with the experiment. The experimental values are estimated from ion spectral-line emission (Al for a temperature of 500 eV and Ti for 1000 eV); the two numbers for each penetration depth are the thicknesses of CH required to reduce the line emission to 10^{-1} and 10^{-3}, respectively, of its value for no CH coating. The second and third columns show the results for flux-limited transport. The last two columns show the result using the delocalization model for the standard and limited delocalization parameters.

Table 27.III
Penetration depth values from heat transport experiments for 1054-nm irradiation, compared with one-dimensional hydrocode simulations. The simulations show results for flux-limited diffusion and for the delocalization model.

		Simulation			
		Flux Limited		Delocalized	
	Experiment	f = 0.1	f = 0.2	λ_H Unlimited	λ_H Limited
200 eV		3.8 μm	4.7 μm	5.0 μm	5.2 μm
500 eV (Al)	6–9 μm	3.6 μm	4.4 μm	4.7 μm	4.9 μm
1000 eV (Ti)	3.5–6 μm	3.2 μm	3.9 μm	3.9 μm	4.2 μm
Absorption	(35 ± 5)%	42%	51%	46%	50%

TC2048

In spite of the substantially higher absorption in the computer simulations (20%–40% higher), the penetration of the 500-eV point on the heat front is far smaller than indicated by the experiment. The delocalized heat front is well characterized by a flux-limited model with f = 0.2. (The effect of limiting λ_H is relatively small.) The delocalized heat front has penetrated about 10% further than the flux-limited front, but this is insignificant compared to the deviation from the experimental results. There is no significant foot on the heat front, as the penetration is into much higher densities ($> 10^{23}$ cm^{-3}) than considered above. This suggests that nonlocal heat transport is not an explanation for the relatively large burn-through depths observed, and that some other process is dominating the penetration of heat into the target.

2. 351-nm Irradiation

Experiments similar to those described above were performed with 351-nm irradiation.[7] The case for a 600-ps FWHM pulse with peak intensity of 8×10^{14} W/cm^2 is considered here. The targets were glass spheres, 150 μm in radius, overcoated with various thicknesses of CH. In this experiment, Si-line emission signaled the penetration of the 500-eV temperature contour, and emission from a Ti substrate signaled the penetration of a 1000-eV temperature.

A summary of the results is shown in Table 27.IV. The penetration depths and laser-absorption fractions for flux-limited transport with f = 0.2 are very similar to those for delocalized transport. The difference between theory and experiment is negligible compared to the 1054-nm experiments.

Table 27.IV
Comparison between penetration depths and absorption from different transport models and experimental data for 351-nm irradiation at 8 × 10^{14} W/cm^2.

		Simulation		
		Flux Limited		Delocalized
	Experiment	f = 0.1	f = 0.2	(λ_H limited)
200 eV		8.5 μm	8.8 μm	9.1 μm
500 eV (Si)	10 μm	8.1 μm	8.6 μm	9.0 μm
1000 eV (Ti)	7–9 μm	7.4 μm	8.4 μm	8.5 μm
Absorption	70%	74%	77%	80%

TC2049

Conclusions

Nonlocal heat transport was investigated under conditions relevant to laser-driven fusion. No significant nonlocal effects were found for irradiation with either 1054-nm or 351-nm laser light. In particular, there was no evidence of a foot on the heat front for full hydrodynamic simulations. The small foot seen in Fokker-Planck simulations at 1054 nm is not genuine because the maximum electron density used was an order of magnitude below solid density. For more realistic density profiles, the higher collisionality from higher density virtually eliminates this effect. Also, the local model cannot accurately replicate the temperature in the very low-density region of the plasma ($n \leq n_c$). Errors in this region do not, however, significantly affect the ablation process and the dynamics of an implosion. Heat flow described by a harmonic-averaged flux limiter between 0.1 and 0.2 appears to be the cannonical result for heat transport in plasmas irradiated with submicron laser light. If a smaller flux limiter is required to explain an experiment, it strongly suggests the presence of additional effects not considered here, such as magnetic fields, turbulence, or multidimensional processes.

ACKNOWLEDGMENT

This work was supported by the U.S. Department of Energy Office of Inertial Fusion under agreement No. DE-FC08-85DP40200 and by the Laser Fusion Feasibility Project at the Laboratory for Laser Energetics, which has the following sponsors: Empire State Electric Energy Research Corporation, General Electric Company, New York State Energy Research and Development Authority, Ontario Hydro, Southern California Edison Company, and the University of Rochester. Such support does not imply endorsement of the content by any of the above parties.

REFERENCES

1. L. Spitzer and R. Härm, *Phys. Rev.* **89**, 977 (1953).

2. J. R. Albritton, *Phys. Rev. Lett.* **50**, 2078 (1983).

3. J. P. Matte, T. W. Johnston, J. Delettrez, and R. L. McCrory, *Phys. Rev. Lett.* **53**, 1461 (1984).

4. J. F. Luciani, P. Mora, and J. Virmont, *Phys. Rev. Lett.* **51**, 1664 (1983); J. F. Luciani, P. Mora, and R. Pellat, *Phys. Fluids* **28**, 835 (1985).

5. J. F. Luciani and P. Mora, GRECO (Ecole Polytechnique) Annual Report No. 91 (1984), p.36.

6. B. Yaakobi, J. Delettrez, L. M. Goldman, R. L. McCrory, R. Marjoribanks, M. C. Richardson, D. Shvarts, S. Skupsky, J. M. Soures, C. Verdon, D. M. Villeneuve, T. Boehly, R. Hutchison, and S. Letzring, *Phys. Fluids* **27**, 516 (1984).

7. B. Yaakobi, O. Barnouin, J. Delettrez, L. M. Goldman, R. Marjoribanks, R. L. McCrory, M. C. Richardson, and J. M. Soures, *Phys. Fluids* **57**, 4354 (1985).

8. J. Delettrez, *Can. J. Phys.* (to be published).

9. Earlier versions of *LILAC* are described in Laboratory for Laser Energetics Reports No. 16 and No. 36 (1976).

10. S. Skupsky, J. Delettrez, and M. Sapir, *Bull. Am. Phys. Soc.* **30**, 1411 (1985).

11. D. L. Book, *NRL Plasma Formulary*, p. 34 (1983).

12. R. J. Langdon, *Phys. Rev. Lett.* **44**, 575 (1980).

13. K. Estabrook and W. L. Kruer, *Phys. Rev. Lett.* **40**, 42 (1978).

Section 3
ADVANCED TECHNOLOGY DEVELOPMENTS

3.A Protective Polymeric Coatings for Nonlinear Optical Materials

Nonlinear optical materials (e.g., KDP and lithium niobate) have become important in high-power laser applications such as frequency conversion and laser Q-switching. The use of these materials, however, has been hampered by the unavailability of antireflective (AR) coatings with high laser-damage resistance and good mechanical and environmental durability. In this article, we shall describe one type of organosilicone resin that has been shown to be useful for the deposition of laser-damage-resistant AR and/or protective coatings on KDP, lithium niobate, and potassium pentaborate. We shall also describe the importance of these polysiloxane resins as an intermediate binding layer for the deposition of multilayer dielectric thin-film AR coatings onto KDP substrates.

The application of damage-resistant evaporated dielectric thin-film coatings onto KDP, KD*P, and lithium niobate has proven difficult. Dielectric thin-film coatings applied directly to KDP substrates are subject to fracture and poor adhesion due to the high coefficient of thermal expansion of KDP,[1] as compared to conventional optical materials such as fused silica and BK-7.[2] In addition, the hygroscopic KDP crystals can be readily damaged by the penetration of moisture through porous AR coatings or coating pinholes. As a result, index matching for KDP frequency-conversion cells has been accomplished by the use of such liquids as propylene carbonate or decalin.

Resorting to an index-matching liquid to reduce Fresnel losses has resulted in complex fluid-filled cell geometries that are subject to

leakage and thermal blooming from refractive-index changes of the fluid caused by localized heating. Recently, an antireflective coating for KDP that makes use of the sol-gel process to deposit a thin, porous layer of silica onto KDP substrates by spin deposition has been reported by Thomas *et al.* at Livermore.[3] Although this coating demonstrated high laser-damage resistance and good optical properties, its extremely poor adhesion allowed it to be readily removed by touching or wiping the coated surface. Additionally, the porous nature of the coating afforded no protection against moisture attack on the KDP substrate.

Potassium pentaborate and deuterated potassium pentaborate have been shown to be useful materials for second-harmonic generation and sum-frequency mixing for wavelengths shorter than 351 nm.[4] The presence of lattice water (or D_2O in the case of the deuterated material) is key in the origin of the nonlinear optical properties of these materials. Exposure of potassium pentaborate to the environment for prolonged periods of time results in loss of lattice water, with a subsequent loss in conversion efficiency and a substantial reduction of the optical quality of the crystals due to surface degradation. As with KDP, a protective coating with high laser-damage resistance and good optical quality would be most desirable.

A different situation holds for the deposition of AR coatings onto lithium niobate. A variety of dielectric thin-film materials that can be readily applied is available;[5] however, the unique physical properties of lithium niobate (ferroelectricity and piezoelectricity) result in temperature-induced surface charging of the material at the elevated temperatures required for evaporated thin-film deposition. This surface charging causes any particulate material present in the coating chamber to be attracted to the substrate and to become imbedded in the AR film during deposition, thus creating sites for laser damage.

Our interest in polysiloxane polymers as potential AR and protective coatings for nonlinear materials was initiated by recent reports[6] of the high laser-damage resistance of one commercially available class of resins manufactured by Owens-Illinois and known as "glass resins." These materials are prepolymerized, high molecular-weight polysiloxane resins that are terminated with silanol end groups and cured by condensation to yield rugged, insoluble coatings of high optical quality. The chemical structure of these polymers is shown in Fig. 27.5. Polysiloxane resins display high optical transmission in the near-IR to near-UV regions of the spectrum. The transmission characteristics of a cured 7-μm layer of a typical polysiloxane resin is shown in Figs. 27.6 and 27.7. The resin is essentially transparent in the 270-nm to 1800-nm region, with a slight improvement in transmission in the UV region after curing.

Earlier experiments performed at LLE[7] and elsewhere[8] have demonstrated the usefulness of polysiloxane resins in producing excellent quality homeotropic alignment in liquid-crystal devices for optical modulation and nonlinear optical applications. Table 27.V summarizes the physical properties of the polysiloxane resins that were used for coating

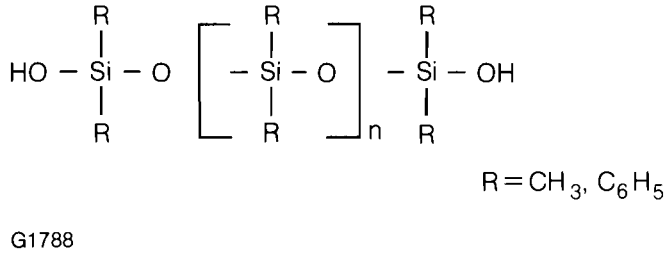

Fig. 27.5
Structure of polysiloxane "glass resin." The refractive index of the polymers is dependent on the organic side groups present (for methyl it is 1.42; methyl and phenyl, 1.43 to 1.55; phenyl, 1.56). The high laser-damage resistance of the polymers is believed to be due to additional purification steps taken during their synthesis.

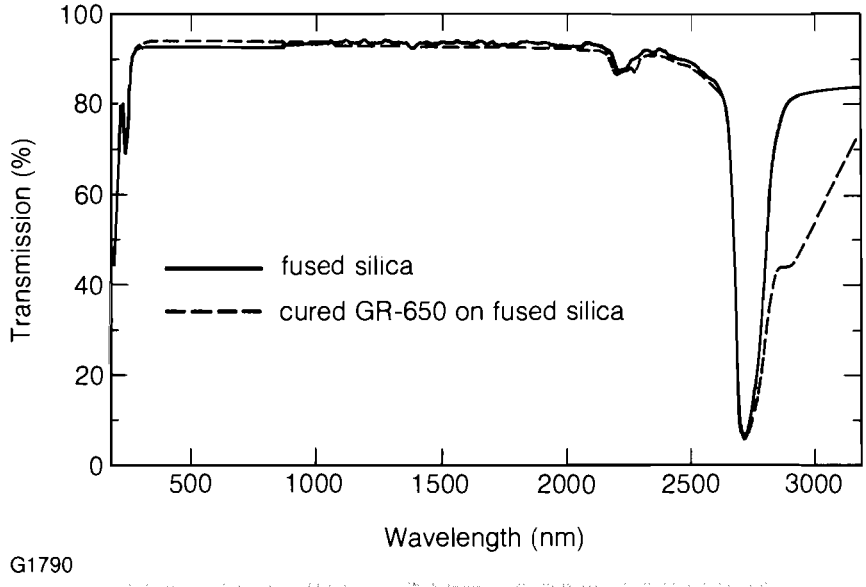

Fig. 27.6
Transmission spectra of fused silica coated on both sides with a 7-μm layer of GR-650 (total path length of polymer: 14 μm) and uncoated fused silica in the near-IR to near-UV region. Substrate thickness: 6.32 mm. The large peak at 2750 nm (fused silica) and the absorption edge at 2800–3000 nm (coating) are due to Si-OH bonds.

experiments with nonlinear optical materials. The availability of polysiloxane resins with refractive indices ranging from 1.42 to 1.56 (589 nm) affords the possibility of creating an index match between the coating and the substrate. This ability to index-match, coupled with the ability to produce particle-free, damage-resistant coatings of high optical quality with relatively simple equipment, made these materials ideal candidates for AR or protective coatings for problem materials such as KDP, lithium niobate, and potassium pentaborate.

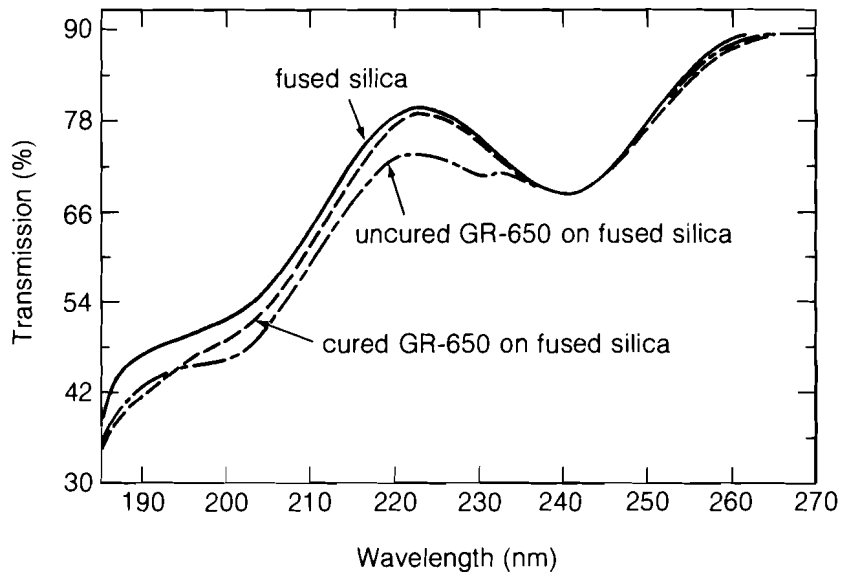

Fig. 27.7
UV transmission spectra of fused silica coated on both sides with a 7-μm layer of GR-650 (total path length of polymer: 14 μm) before and after coating at 120°C for 24 hours. Also displayed is the transmission of the fused silica substrate (6.32-mm thick) before coating. An increase in transmission of the coating in the UV region after curing is evident.

Table 27.V
Physical properties of Owens-Illinois polysiloxane resins.

Resin	Organic Side Group	% Solids Content	Refractive Index (589.6 nm)	Refractive Index (1064 nm)	Cure Temp/ Time
GR-650	methyl	100	1.42	1.4028	120°C/24 h
GR-651	methyl	27.5 (butanol)	1.42	---	120°C/0.5 h
GR-100	methyl-phenyl	100	1.49	---	120°C/24 h

G1810

In the following sections, the coating experiments performed and the results obtained are described as they pertain to each of the nonlinear optical materials investigated.

Coatings for KDP and KD*P

1. KDP

Samples used for the KDP coating experiments were supplied by Inrad. The disk samples supplied were 50-mm diameter by 6.3-mm thick (scratch-dig 100/25), Type 2 cut, which had been polished by conventional means. All cleaning and coating operations were performed under Class 100 clean-room conditions in a horizontal laminar-flow hood. The initial coating experiments that were conducted with KDP used GR-651 polysiloxane resin, supplied precatalyzed as a 27.5% solution in butanol. Early results with this material indicated that it was too brittle in its fully cured state to withstand the mechanical stresses caused by the thermal expansion and contraction of KDP. Coatings prepared with this material were found to crack upon cooling after the bake cycle or when exposed to moisture. A potential solution to this problem was to use the uncatalyzed GR-650 resin, which was expected to be more flexible than GR-651 because of its lower degree of cure. This resulted in a lower glass-transition temperature for the polymer. The validity of this approach was confirmed by the successful spin deposition of an 0.8-μm film of GR-650 polysiloxane resin on a KDP substrate using a 3% solution of GR-650 resin in isopropanol. No cracking of the coating upon exposure of the coated KDP part to moisture was noticed. The interferometric quality of the KDP substrate, measured with a Zygo Mark II Interferometer at 633 nm, was unchanged by the presence of the coating.

2. KD*P

A sample of KD*P, 10 × 10 × 5-mm thick (95% deuterated) from Cleveland Crystals Co., which had been finished by diamond turning, was coated with a 3% solution of GR-650 polysiloxane resin in isopropanol under the same conditions used for the conventionally polished samples from Inrad. There appeared to be no appreciable difference in the behavior of KD*P and KDP toward the spin-coating technique used in the coating experiments.

3. Evaporative Thin-Film Overcoating of Polysiloxane-Coated KDP

Two Inrad KDP substrates that had been previously coated on one side with GR-650 polysiloxane resin were overcoated with a Ta_2O_3-SiO_2 multilayer evaporated thin film to produce a durable broadband AR coating. The AR coating was designed to accommodate the uncertainty in thickness of the polysiloxane layer. Prior to deposition of the thin-film coating, a small portion of the polysiloxane film near the edge of each sample was removed by rubbing with a cotton swab soaked in methanol. The exposed area on both samples was overcoated with a thin film of aluminum to aid in visualization of the KDP surface by Nomarski differential-interference contrast microscopy. One of the substrates was overcoated with the dielectric thin-film material, by e-beam evaporation at 150°C. Visual inspection of the overcoated KDP crystal after coating revealed a foggy texture over most of the coated

surface, with the exception of some clear areas near the center of the piece. Detailed observation of the sample by Nomarski microscopy revealed that the fogginess was due to buckling of the polysiloxane underlayer (see Fig. 27.8) in a manner indicating high compressive stress. The polysiloxane/dielectric thin-film composite coating was exceptionally well adhered to the KDP substrate. The coating passed the "Scotch-tape" test and could only be removed with difficulty by scratching with a sharp knife. Attempts to remove the coating by wiping with a cotton swab soaked in methanol were unsuccessful. A second coating run at a lower temperature (100°C) was made. In this case no buckling of the polysiloxane underlayer was noted; however, the coating-to-substrate adhesion was considerably reduced, compared to the earlier high-temperature run. The coating was readily removed with the tape test. The surface quality of the dielectric thin-film polysiloxane-coated KDP substrate is revealed in Fig. 27.9. The surface roughness of the substrate appears to be reduced by the presence of the composite coating.

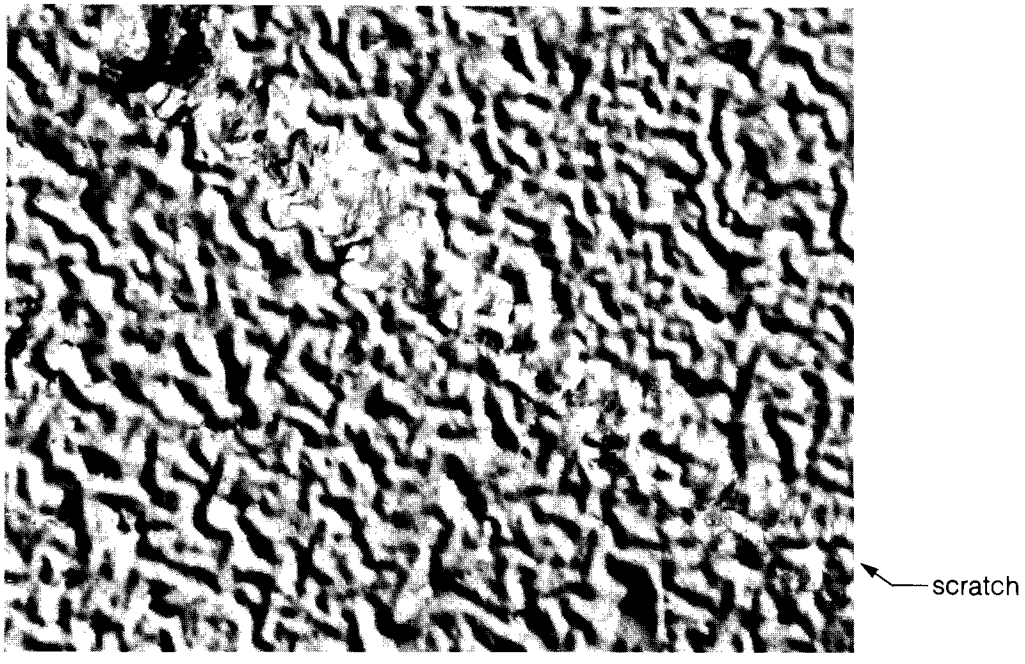

G1792

Fig. 27.8
Polysiloxane-coated KDP overcoated with evaporated AR film at 150°C (magnification: 375x). The buckling of the polysiloxane underlayer is evidence of compressive stress caused by the high thermal expansion of the substrate at 150°C and the rigidity of the evaporated AR film. Adhesion of the composite film is excellent; the coating could only be removed with difficulty by scratching with a sharp knife.

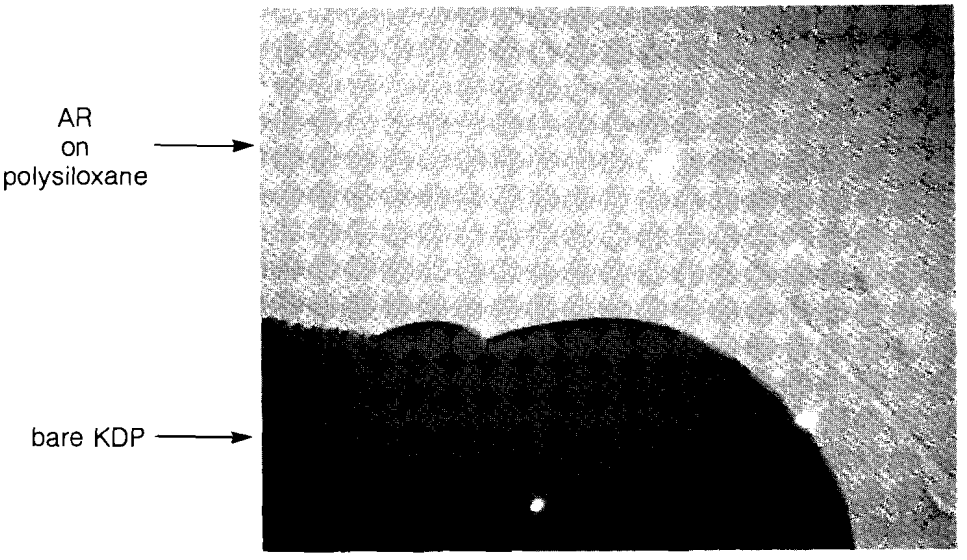

G1793

Fig. 27.9
Polysiloxane-coated KDP overcoated with evaporated AR film at 100°C. No buckling due to compressive stress is indicated. Adhesion of the composite film is poor. The area where the coating was removed by the "Scotch-tape" test is indicated in the lower portion of the photograph. A smoothing effect produced by the AR-PSX coating is evident (magnification: 750x).

4. Damage Testing Data: Coated KDP Samples

The coated samples of KDP and KD*P described earlier were subjected to some preliminary damage tests at 1064 nm. The results and experimental conditions for the tests are summarized in Tables 27.VI–27.VIII.

All of the polymer-coated samples displayed excellent damage test results, exceeding in some cases the damage threshold of the AR-coated BK-7 control. Application of the dielectric thin-film coating over the polymer coating, however, caused a substantial reduction in the damage threshold of the composite coating.

Table 27.VI
CW irradiation of GR-650 polysiloxane-coated KDP (tested at LLE).

Sample No.	1
Sample Description:	KDP, coated both sides with a 7-μm layer
Laser:	1-W cw Nd:YAG
Spot Size:	0.5 mm
Intensity:	400 W/cm^2
Irradiation Time:	10 min
Result:	no damage (100x microscopic observation)

G1811

Table 27.VII
*Pulsed irradiation of GR-650 polysiloxane-coated KD*P (tested at General Electric Co.).*

Sample No.	2
Sample Description:	diamond-turned KD*P, coated on one side
Laser:	Nd:YAG, 1064 nm
Beam Size:	6 mm × 0.7 mm (measured with burn paper)
Pulse Width:	18 ns
Maximum Energy/Pulse:	240 mJ
Repetition Rate/Time:	5 KHz/1 min
Result:	no damage
Calculated Intensity	309 MW/cm^2
Calculated Fluence:	5.6 J/cm^2

G1812

Table 27.VIII
Pulsed irradiation of dielectric thin-film polysiloxane-coated KDP (tested at Inrad).

Sample No.	3	
Sample Description:	KDP coated on one side with GR-650 polysiloxane resin, partially overcoated with a dielectric thin film	
Laser:	Nd:YAG (1064 nm)	
Pulse Width:	15 ns	
Number of Shots	100 per site, 6 sites per sample	
Results:	Material	Relative Damage Threshold
	AR-coated BK-7 control	1.0 (300 MW/cm^2)
	Polysiloxane-coated KDP	1.12
	Polysiloxane-dielectric thin-film-coated KDP	0.43

G1813

Coatings for Lithium Niobate

To coat lithium niobate with a single-layer AR film, the refractive index of the coating material at 1064 nm must be 1.48, as calculated from the equation

$$n_1 = (n_o)^{1/2} , \quad (1)$$

where n_1 is the index of coating and n_o is the index of substrate. For lithium niobate, the average refractive index at 1064 nm is 2.1.

The particular polysiloxane resin selected for this task was GR-100 for the close match of its refractive index (1.49 at 589 nm) to the required value. The transmission characteristics of the GR-100 polysiloxane resin are similar to those of GR-650, demonstrating high transparency between 270 and 1800 nm with a slight increase in UV transparency after curing. The coating thickness required to produce a perfect AR effect at 1064 nm (zero-order interference) was calculated from the formula

$$\lambda_{min} = \frac{4n_1 t}{2m+1} , \quad (2)$$

where m is here 0, λ = 1064 nm, and n_1 = 1.48. The resulting value for the coating thickness (t) was 1800 Å.

Samples of lithium niobate used in the coating experiments were 10 × 10 × 2-mm thick plates provided by Inrad. Because of the unique physical properties of lithium niobate (the material is ferroelectric, piezoelectric, and undergoes temperature-induced surface charging) great care was required in handling, cleaning, and coating this material. As with the KDP coating experiments, all of the cleaning and coating operations were conducted in the horizontal laminar-flow hood under Class 100 clean-room conditions.

1. Coating Experiments: Lithium Niobate

Antireflective coatings formed from GR-100 polysiloxane resin were applied to the lithium niobate samples by spin deposition, using the procedure that was developed for KDP. The optimal solution concentration required to produce a polysiloxane coating of approximately 1800 Å was determined by spin coating three lithium niobate substrates with 3%, 6%, and 12% solutions of GR-100 polysiloxane resin in isopropanol and determining the transmission characteristics of the samples with the Perkin-Elmer Lambda 9 UV-VIS-NIR spectrophotometer. The results indicated that the 3% solids coating appeared to be the most likely candidate for producing a broadband AR coating at 1064 nm. One lithium niobate crystal was spin coated with the 3% solution of GR-100 in isopropanol and baked at 120°C for 24 hours to cure the coating. An additional substrate was coated on both sides with GR-100 polysiloxane resin by sequentially coating and baking each side of the substrate. In Fig. 27.10, the transmission characteristics of the single-side coated/baked, double-sided coated/baked, and uncoated lithium niobate samples are compared. A gain of about 8% in transmission at 1μm was achieved by coating one side; coating both sides of the substrate increased the transmission at 1μm to nearly 95%.

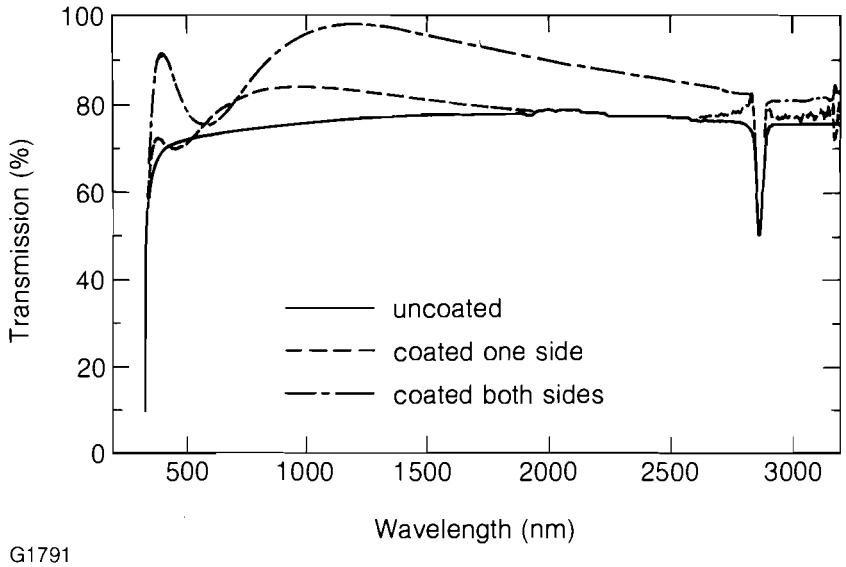

Fig. 27.10
Transmission spectra of polymer AR-coated lithium niobate samples and an uncoated control. Coating both sides increased transmission to nearly 95%.

2. Damage Test Data: Lithium Niobate

Damage testing of the polysiloxane-coated lithium niobate substrates was carried out at Inrad. As in earlier damage testing experiments with coated KDP, an AR-coated BK-7 substrate was used as a control sample and a relative damage threshold of 1.0 was assigned to the test results on this sample. The damage-test conditions and results are presented in Table 27.IX. The low damage resistance obtained for the polysiloxane-coated lithium niobate samples could be due to poor initial surface quality of the substrates before coating. It should be pointed out that although the laser-damage resistance of the GR-650 resin that was used for KDP coatings has been well documented, no data exists on the damage resistance of the GR-100 resin that was used in these experiments. Since an uncoated sample of lithium niobate was not available for damage testing, it was not possible to determine the degree of protection, if any, that was afforded by the presence of the polysiloxane coating.

Coatings for Potassium Pentaborate

Several samples of potassium pentaborate (10 × 11 × 5.5-mm thick) were received from Inrad for coating with a polysiloxane layer intended to protect the polished surfaces from degradation due to loss of lattice water to the environment. The samples had been polished on only two of the four narrow faces. One sample was left uncoated as a control; a second sample was prepared for coating by bonding a glass capillary tube to one of the narrow unpolished faces with an epoxy adhesive. The sample was secured by the capillary tube and was dipped in a 3% solids solution of GR-650 in isopropanol. After air drying, the sample was baked at 120°C for 24 hours. The coated and uncoated samples were photographed at 160x (Nomarski) to qualify the surface conditions

Table 27.IX
Pulsed irradiation of GR-100 polysiloxane-coated lithium niobate (tested at Inrad).

Sample Description	lithium niobate crystals, one piece coated on one side only, second piece coated on both sides	
Laser:	Nd:YAG (1064 nm)	
Pulse Width:	15 ns	
Number of Shots	100 per site, 6 sites per sample	
Results:	Material	Relative Damage Threshold
	AR-coated BK-7	1.00 (300 MW/cm^2)
	Goal for AR on $LiNbO_3$	0.63
	Polysiloxane-coated $LiNbO_3$ (1 pc, 1 side)	0.24
	Polysiloxane-coated $LiNbO_3$ (2 pc, 1 side)	0.26
	Polysiloxane-coated $LiNbO_3$ (2 pc, 2nd side)	0.30

G1814

before exposure to the atmosphere (Figs. 27.11 and 27.12). The nodules that appear on the surface of the coated parts result from poor wetting of the KPB surface by the coating solution. The samples were placed in the laminar-flow hood, with the polished surfaces parallel to the laminar air-flow direction, and allowed to stand exposed to a constant flow of air for eight days. Examination of the samples under the microscope showed that the surface of the uncoated sample had become pitted (Fig. 27.13) and the coated sample was unchanged (Fig. 27.14). The experiment was continued for an additional six days and the pieces were reexamined. The uncoated piece had deteriorated to the point that the surface damage was visible to the unaided eye. The coated sample remained unchanged after a total of 14 days' exposure to the atmosphere.

The Owens-Illinois polysiloxane resins have been demonstrated to be potentially important materials for use as antireflective or protective coatings for certain nonlinear optical materials. Considerable effort involving the optimization of coating process conditions remains to be undertaken. One of the areas that requires attention is the optimization of dielectric thin-film deposition conditions for overcoating of polysiloxane-coated KDP to increase adhesion, improve optical quality, and increase the damage threshold of the composite coating. The effect of initial surface condition on the laser-damage resistance of polymer-coated lithium niobate crystals should also be investigated. For potassium pentaborate, optimum coating conditions and damage resistance of polysiloxane-coated substrates have yet to be determined. A natural extension of this work with polysiloxane resins would be the coating of urea and other nonlinear optical materials that have been difficult or impossible to coat by conventional means.

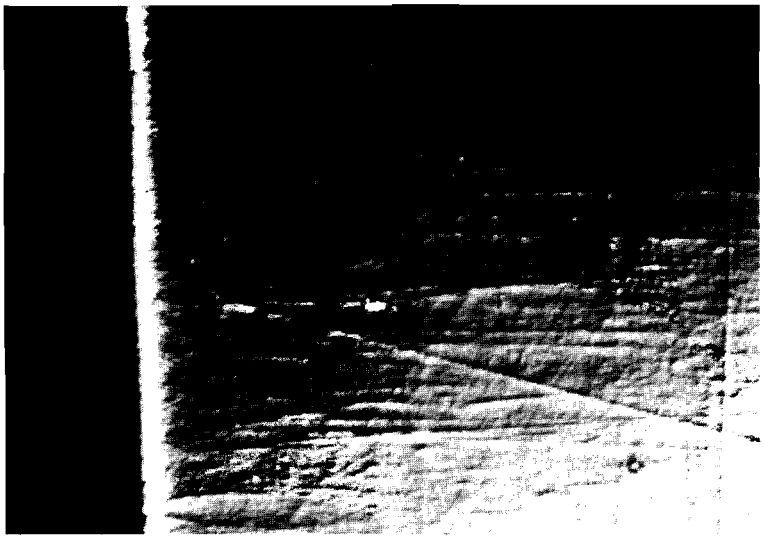

G1794

Fig. 27.11
Uncoated potassium pentaborate control sample (magnification: 160x). Surface condition at the beginning of experiment. Surface scratches as a result of polishing are evident.

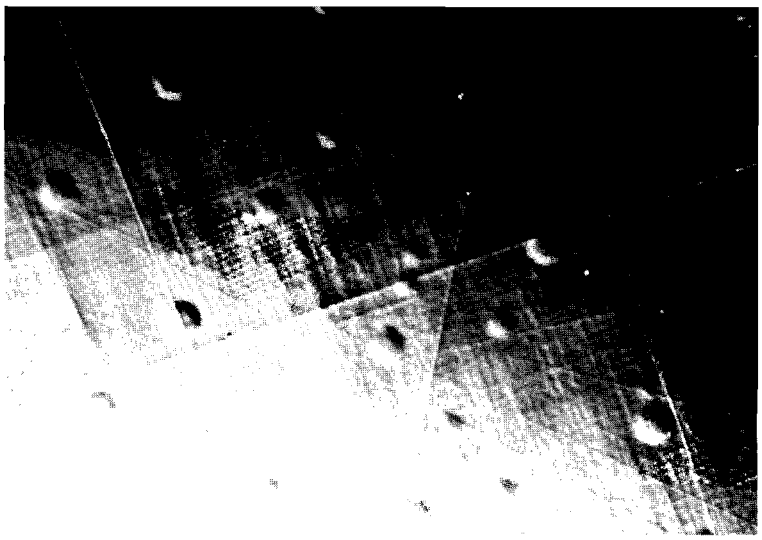

G1795

Fig. 27.12
Potassium pentaborate sample dip-coated with a 3% solution of GR-650 polysiloxane resin in isopropanol. The photo indicates the surface condition at the beginning of experiment. Nodules, high spots in the coating, are due to poor wetting of the surface by the coating solution.

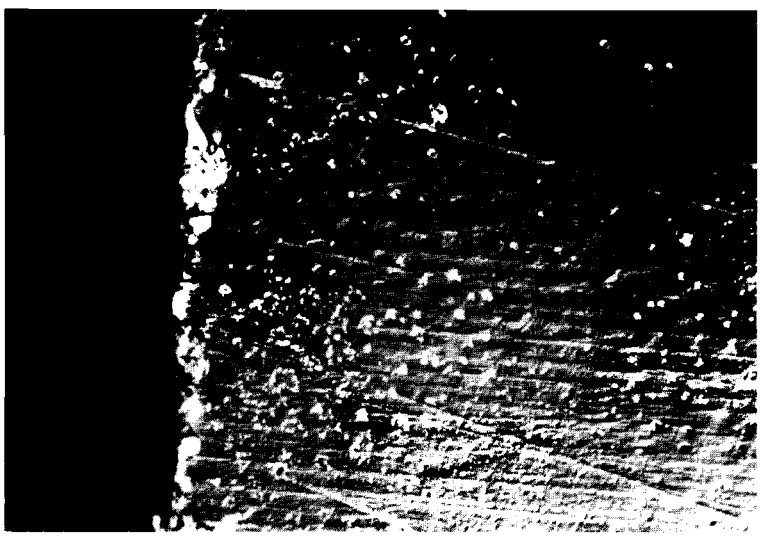

G1796

Fig. 27.13
Uncoated potassium pentaborate control sample after eight days' exposure to air (magnification: 160x). The surface quality is considerably degraded due to loss of lattice water.

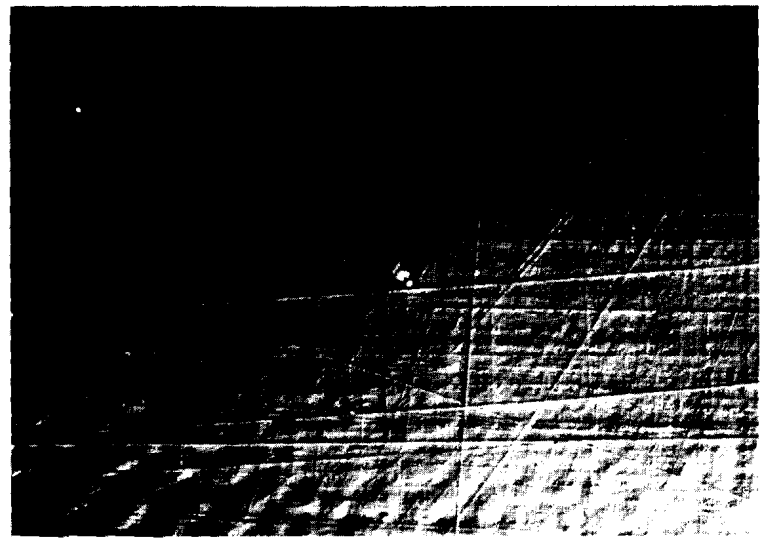

G1797

Fig. 27.14
Coated potassium pentaborate sample after eight days' exposure to air (magnification: 160x). The surface quality is essentially unchanged, indicating the effectiveness of the polysiloxane coating as a moisture barrier.

ACKNOWLEDGMENT

This work was supported by the General Electric Company Advanced Laser Technology Group, Binghamton, NY, under contract No. A25-E-0580BS, the New York State Center for Advanced Optical Technology of the Institute of Optics, the U.S. Department of Energy Office of Inertial Fusion under agreement No. DE-FC08-85DP40200, and by the Laser Fusion Feasibility Project at the Laboratory for Laser Energetics, which has the following sponsors: Empire State Electric Energy Research Corporation, General Electric Company, New York State Energy Research and Development Authority, Ontario Hydro, Southern California Edison Company, and the University of Rochester. Such support does not imply endorsement of the content by any of the above parties.

The author also gratefully acknowledges Owens-Illinois Company, Toledo, OH, for supplying samples of materials for experimentation; Ian Thomas, Lawrence Livermore National Laboratory, for helpful discussions; Inrad Inc., Northvale, NJ, for samples of nonlinear optical materials and damage testing; and Bruce Boczam, General Electric, for damage testing of KD*P.

REFERENCES

1. J. T. Milek and M. Newberger, *Handbook of Electronic Materials* (IFI-Plenum), Vol. 8, p. 177.
2. *Schott Handbook of Optical Glasses*, Jena^{er} Glasswerk Schott and Gen., Mainz (West Germany).
3. I. M. Thomas, J. G. Wilder, W. H. Lowdermilk, and M. C. Staggs, "High Damage Threshold Porous Silica Antireflective Coating," presented at the Boulder Damage Symposium, Boulder, CO, 15-17 October 1984.
4. J. A. Paisner, M. L. Spaeth, D. C. Gerstenberger, and I. W. Ruderman, *Appl. Phys. Lett.* **32**, 476 (1978).
5. M. S. Soileau, *Appl. Opt.* **20**, 1030 (1981).
6. I. Thomas, "Frequency Conversion for High Power Lasers," Technology Transfer Symposium, 13-14 June 1985, LLNL.
7. K. L. Marshall, *Mol. Cryst. Liq. Cryst. Lett.* **3**, 133-138 (1986).
8. D. Armitage and J. I. Tackara, "Liquid Crystal Differentiating Spatial Light Modulator," SPIE, 0-E LASE'86 Conference 613: Nonlinear Optics and Applications, 19-24 January 1986, Los Angeles, CA.

3.B Time-Resolved Observation of Electron-Phonon Relaxation in Copper

The 1-KHz, synchronously amplified, colliding-pulse, mode-locked[1] laser at LLE is currently being used to study ultrafast phenomena in solid-state materials. Transient thermal modulation of the optical properties of metals is under investigation with the goal of time-resolving electron relaxation kinetics.[2]

Thermal modulation of the optical properties of metals is a widely used technique in studying critical points in band structure. Recently the modulation of reflectivity of copper has been used to observe nonequilibrium electron-lattice temperatures during picosecond (~ 5-ps FWHM) laser heating of up to a few degrees.[3] Although nonequilibrium heating was demonstrated in these experiments, the time resolution was insufficient to resolve electron-phonon relaxation. In a subsequent report, the phenomenon of thermally enhanced multiphoton photoemission was used to time resolve electron-phonon relaxation in tungsten.[4] Results indicated that such relaxation is accomplished in a few hundred femtoseconds. Using amplified, 150-fs to 300-fs laser pulses, we have time resolved electron-phonon relaxation by monitoring the laser-heating-induced modulation of the transmissivity of 200-Å copper films.

A 1-KHz, synchronously amplified, colliding-pulse, mode-locked laser ($\lambda \sim 620$-nm) was used for the pump-probe experiments. The sample was heated by using the 620-nm fundamental laser frequency. Probing was accomplished at 620 nm or by using a 10-nm (FWHM) band from white light, generated by focusing the probe beam on an ethylene-glycol cell. The pump and probe were incident collinearly, normal to the copper film (polarized perpendicular to each other), and focused to ~ 27-μm- and ~ 14-μm-diameter spots respectively, such that the probe was near the center of the pump.

The transmissivity of the thin copper films at $\lambda \sim 620$ nm during laser heating (~300-fs FWHM), for a pump laser fluence of 15 nJ (a) and 65 nJ (b), is shown in Fig. 27.15. The initial transmitted signal appears to integrate the heating pulse. The decay of the fast transient was found to be 1–4 ps and to increase with the heating pulse fluence. This effect is due to larger differences between electron and lattice temperatures for higher fluences, where more electron-phonon collisions are required for thermalization.

A simplified numerical model of nonequilibrium heating of copper was constructed and applied to the conditions in Fig. 27.15. This model is based on a solution of two coupled nonlinear differential equations in the form[3,4]

$$C_e(T_e)\frac{dT_e}{dt} = P_o(t) - G(T_e - T_\ell) , \quad (1)$$

$$C_\ell \frac{dT_e}{dt} = G(T_e - T_\ell) . \quad (2)$$

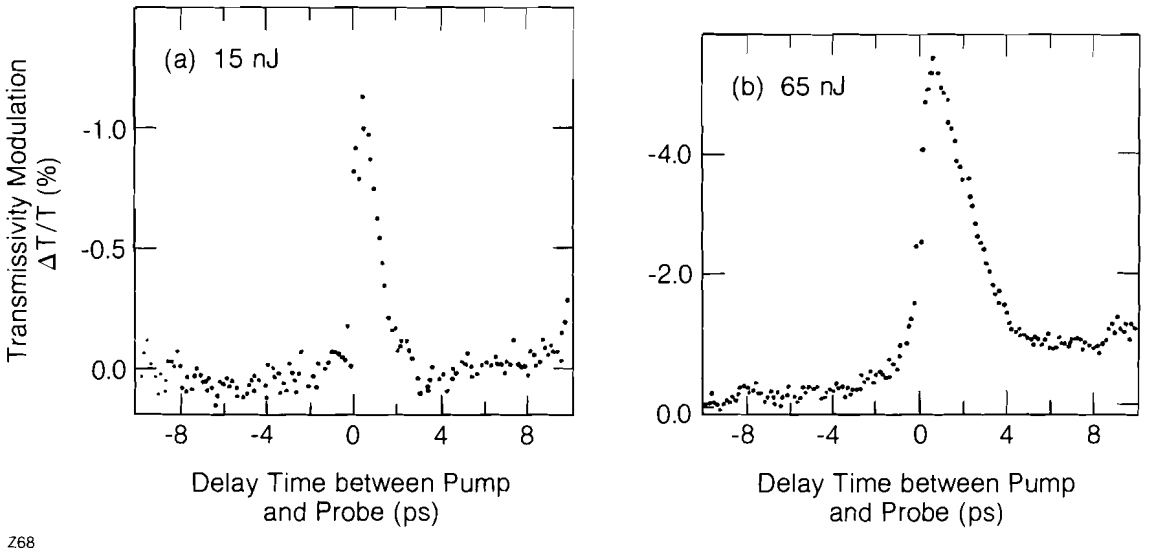

Fig. 27.15
Time-resolved transmissivity of 200-Å copper film during laser heating (~300-fs FWHM at λ ~ 620 nm). Pump and probe focused to ~27-μm- and ~14-μm-diameter spots, respectively.

Here, $C_e(T_e)$ is the electronic heat capacity, which is directly proportional to the electron temperature; $P_o(t)$ represents the laser heating pulse; and G is the electron-phonon coupling constant. Thermal conductivity losses were ignored due to the thin-film geometry used in the present work. Simulation of conditions used in Fig. 27.15, for different values of electron-phonon coupling constant G, are shown in Fig. 27.16. Results indicate that G has a value of $\sim 1 \times 10^{17}$ W/(m^{3}K). For a pulse energy of 65 nJ (peak fluence $\sim 3.8 \times 10^{10}$ W/cm^2), the model predicts a peak electron temperature of 2200°K and an equilibrium electron-phonon temperature of 385°K.

Using white light in 10-nm spectral-band steps from λ = 560 nm to 640 nm (λ = 590 nm corresponds to an electron transition from the top of the d-band to the Fermi level) showed similar behavior as when probing at λ = 620 nm.

In summary, we have directly measured the electron-phonon relaxation time in copper as a function of pump-laser fluence and probe photon energy, for λ = 560 nm to 640 nm. We have demonstrated nonequilibrium heating with a large (few thousand degrees) difference between electron and lattice temperatures. Electronic and lattice effects on the optical properties of copper were separated in time. Extension of probe measurements to the near-IR and UV parts of the spectrum would serve to separate effects of bound and free electrons on the optical properties and provide considerable information on the band structure.

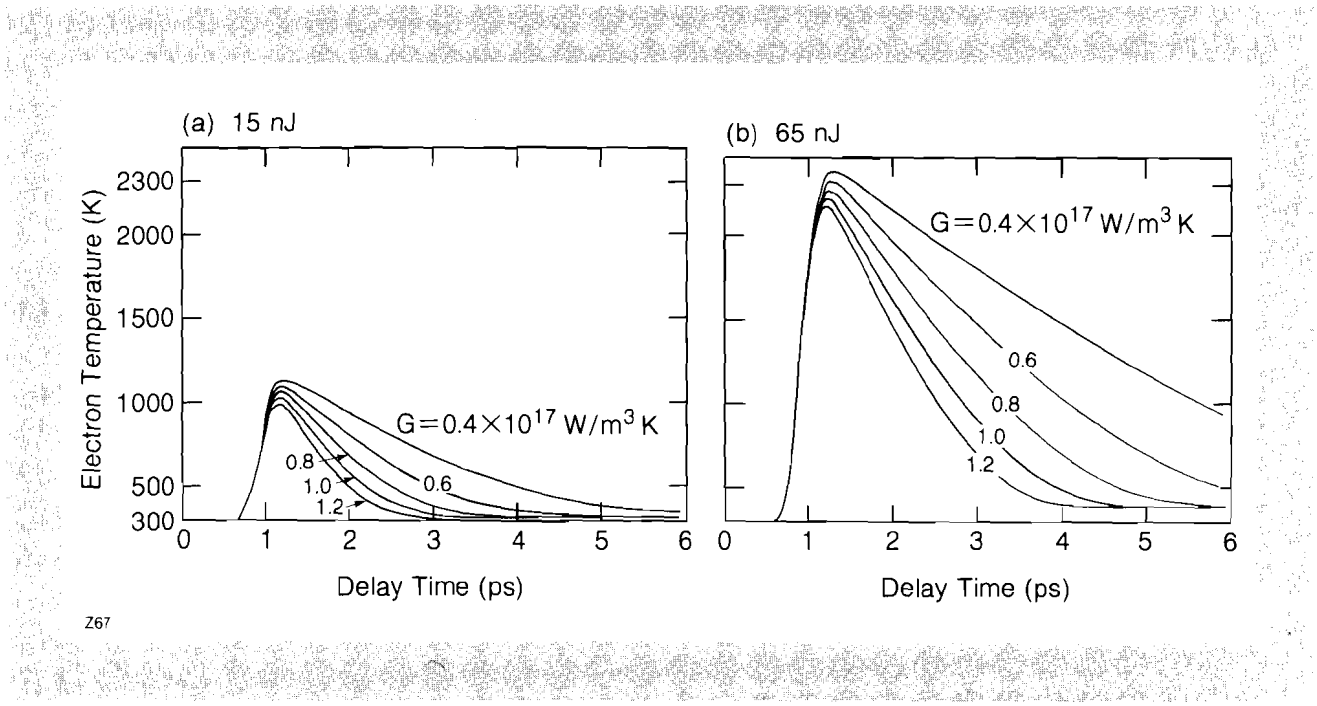

Fig. 27.16
Numerical modeling of the time evolution of electron temperature for the experimental condition of Fig. 27.15. Simulations were made for different values of the coefficient of heat transfer between the electrons and the lattice G.

ACKNOWLEDGMENT

This work was supported by the Laser Fusion Feasibility Project at the Laboratory for Laser Energetics, which has the following sponsors: Empire State Electric Energy Research Corporation, General Electric Company, New York State Energy Research and Development Authority, Ontario Hydro, Southern California Edison Company, and the University of Rochester. Such support does not imply endorsement of the content by any of the above parties.

REFERENCES

1. I. N. Duling III, T. Norris, T. Sizer II, P. Bado, and G. A. Mourou, *J. Opt. Soc. Am. B* **2**, 616 (1985).
2. H. Elsayed-Ali, M. Pessot, T. Norris, and G. Mourou, in *Ultrafast Phenomena*, Vol. V, edited by T. Siegman and G. Fleming (Springer-Verlag, Heidelberg, to be published).
3. G. L. Eesley, *Phys. Rev. Lett.* **51**, 2140 (1983).
4. J. G. Fujimoto, J. M. Liu, E. P. Ippen, and N. Bloembergen, *Phys. Rev. Lett.* **53**, 1837 (1984).

3.C Noncontact Electro-Optic Sampling with a GaAs Injection Laser

Due to high cost and large size of dye-based short-pulse laser systems, the application of electro-optic sampling to the measurement of high-speed electrical waveforms has been limited to a small number of research laboratories. This is unfortunate, as it means that the advantages of electro-optic sampling over direct electronic sampling are not being fully exploited. Those advantages are a very high-speed reserve (up to a few THz) and the possibility of noninvasive electric field measurement.

Here we describe an electro-optic sampling system that is compact, uses a semiconductor laser source, and supports a versatile, substrate-independent probing geometry (Fig. 27.17).

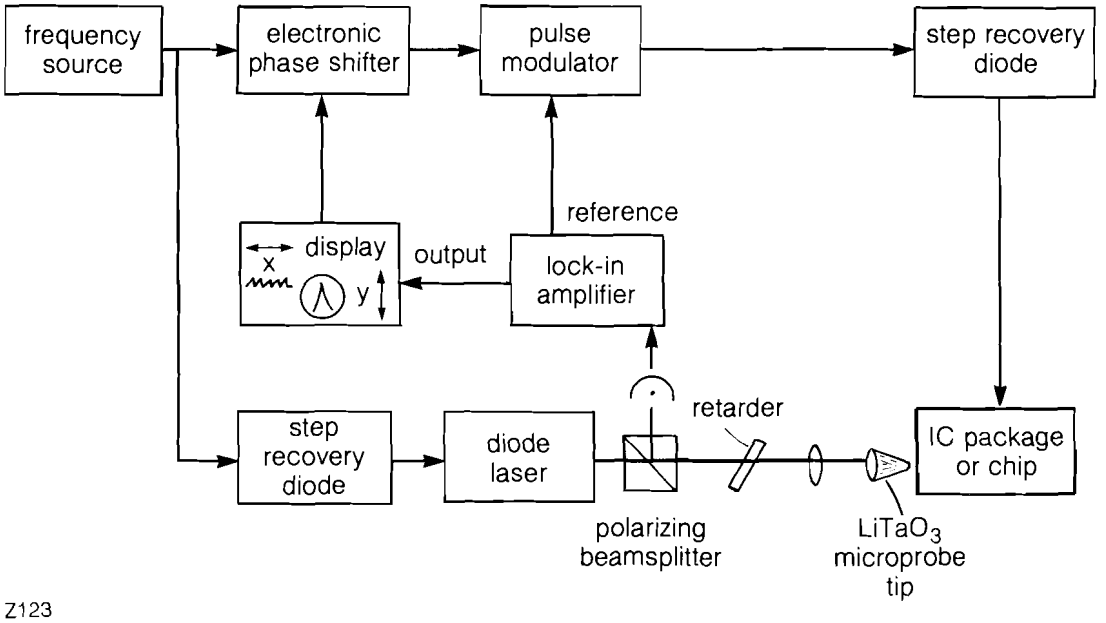

Fig. 27.17
Schematic of electroc-optic sampler with a finger probe.

The repetition rate of this system is set by a 100-MHz oscillator (though all of the system components allow greater than 1-GHz repetition rate). About 1 W of the oscillator power is used to drive a step-recovery-diode-based comb generator (Hewlett-Packard), which in turn pulses a current-biased GaAs injection laser. These 830-nm pulses (Fig. 27.18) have been time resolved on a streak camera showing less than 30-ps FWHM and a very low background level.

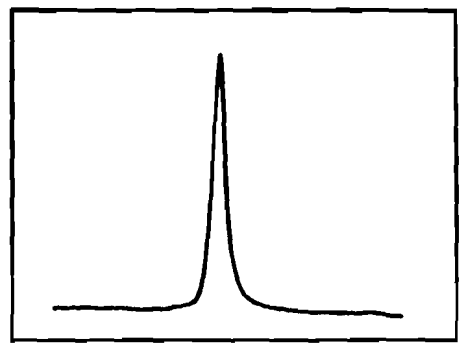

30-ps laser diode pulses displayed on a streak camera

Z45

Fig. 27.18
Streak camera trace of 30-ps laser-diode pulses.

The delay necessary to scan the sampling point in time is provided by an electronic phase shifter in a second branch off the main oscillator. This device is more flexible and less expensive than the optical delay lines or two-frequency phase controllers normally used. Finally, a reflective-mode Pockels cell is used as an electro-optic modulator to provide a substrate-independent, versatile geometry for testing devices and packages. This "finger probe" (Fig. 27.19) is a small cone of electro-optic material with a very small, high-reflectivity-coated flat[2] on the tip. In use, the probe is brought near an operating electronic circuit so that the tip is immersed in the circuit's fringing fields. With all these components in place, a polarized train of short optical pulses is focused down through the back of the cone onto the tip, where the electric field induces a change in the polarization, linear with its intensity. After the light retroreflects off the high-reflectivity coating, it passes back through the optics where it is subsequently detected by a PIN photodiode and processed, using lock-in techniques. Although our experiment uses 30-ps optical pulses to sample electric fields, we could also use 100-fs pulses from dye laser sources to measure much faster phenomena because the electro-optic crystal can be transparent in the visible. This probing geometry is also compatible with the use of UV light, where submicron spot size could lead to very fine spatial resolution.

In our experiment, a small section of the ground conductor of a semirigid coaxial cable was removed and the finger probe immersed in the electric fields bridging the center conductor and the remaining outer conductor. The feedthrough from the cable was also sampled with a Tektronix sampler. These results (Fig. 27.20) agree to within 10% in time. The finger-probe "pocket" sampler has also been used to measure the fields around IC packaging pins, the fields of intrapackage connections, and the fields around package-to-chip wire bonds, as well as signal propagation and cross-talk on, and as far as 400 μm above, an alumina test structure.

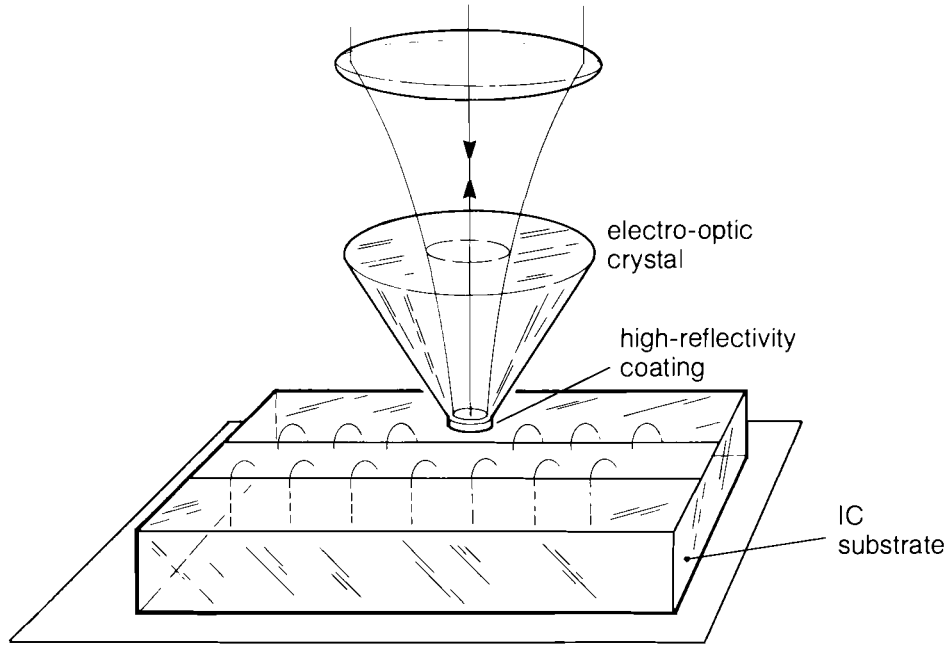

Fig. 27.19
Electro-optic "finger probe."

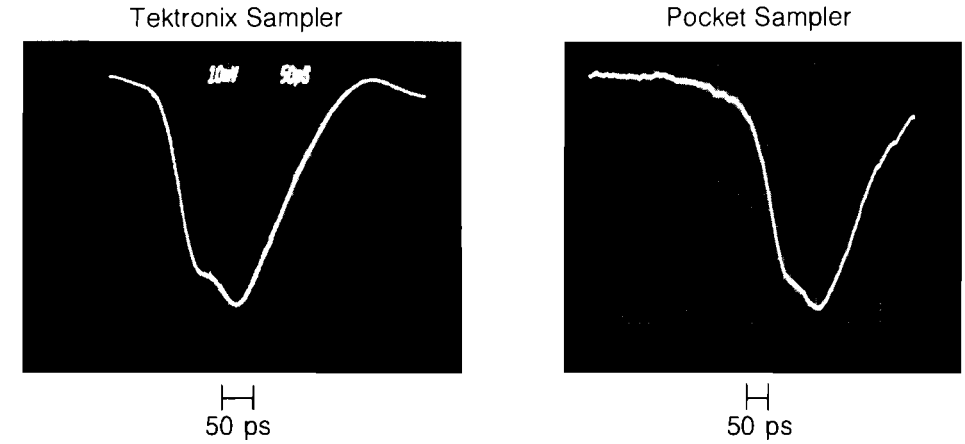

Fig. 27.20
Comparison of electronic (Tektronix) and electro-optic samplers.

In conclusion, the ability to make noncontact measurements of electrical waveforms with 30-ps laser-diode pulses, an electronic phase shifter, and a versatile, substrate-independent probe have been demonstrated. With the availability of this inexpensive electro-optic sampling technology and the trends toward shorter pulses from semiconductor sources, it is hoped that electro-optic sampling will become available to the ordinary electronics laboratory.

ACKNOWLEDGMENT

We wish to express our thanks to Steve Williamson and Greg Sucha for their contributions to the development of this system.

This work was supported by the Laser Fusion Feasibility Project at the Laboratory for Laser Energetics, which has the following sponsors: Empire State Electric Energy Research Corporation, General Electric Company, New York State Energy Research and Development Authority, Ontario Hydro, Southern California Edison Company, and the University of Rochester. Such support does not imply endorsement of the content by any of the above parties.

REFERENCES

1. J. A. Valdmanis, G. A. Mourou and C. W. Gabel, *Appl. Phys. Lett.* **41**, 211–212 (1982).
2. K. E. Meyer and G. A. Mourou, in *Picosecond Electronics and Optoelectronics* (Springer-Verlag, Berlin, Heidelberg, New York, and Tokyo, 1985), pp. 54–57.

Section 4
NATIONAL LASER USERS FACILITY NEWS

NLUF activities during the third quarter of FY86 included five series of experiments on OMEGA and notification of Principal Investigators of the NLUF Steering Committee's evaluation of new proposals.

J. Seely, U. Feldman, and **C. Brown** of the Naval Research Laboratory (NRL) and **W. Behring** of the NASA-Goddard Space Flight Center concluded their investigations of XUV and x-ray spectroscopy of high-Z ions. Targets of Au (Z = 79), Pb (Z = 82), Th (Z = 90), and U (Z = 92) were irradiated with the OMEGA laser. This is an extension of previous work to much higher-Z ions.

H. Griem from the University of Maryland conducted experiments on thermal transport of spherical laser targets. This experiment used glass and CH microballoons with a Ti layer embedded in the target. XUV and x-ray spectra were measured to determine the heating of OMEGA-irradiated targets.

D. Duston of SDIO and NRL and **A. Hauer** of Los Alamos National Laboratory (LANL) collaborated with LLE scientists and concluded the experiments on dielectronic satellites of Ar x-ray line emission from compressed targets. The glass targets, fabricated at LANL, are filled with Ar and D_2 and then overcoated with several microns' thickness of CH. Time-integrated and time-resolved spectra of the x-ray emission and absorption were obtained.

P. G. Burkhalter and **J. Reader** of NRL concluded the measurement of x-ray spectra from high-Z targets. X-ray emission from Fe, CeO, Ta, BaF, HaF, Te, and W targets were recorded with a curved crystal spectrograph. These data are now being analyzed at NRL.

U. Feldman and **C. Brown** of NRL have collaborated with LLE scientists to implement a spectro-heliograph on the OMEGA target chamber. This instrument records spectral images of the irradiated target at x-ray line emission from 186 Å to 400 Å. Images were obtained for several CH and glass microballoons. Although preliminary, the data indicate that this instrument will prove a valuable tool for looking at XUV emission from implosion targets.

The NLUF Steering Committee reviewed 15 proposals for FY87. Nine of the 15 were recommended for facility time, and eight of the nine were recommended for DOE funding.

Proposals for consideration for the FY88 funding cycle are due by 15 December 1986.

For more information regarding proposal guidelines and the resources available at the National Laser Users Facility, please contact:

Manager
National Laser Users Facility
Laboratory for Laser Energetics
University of Rochester
250 East River Road
Rochester, New York 14623-1299
(716) 275-2074

ACKNOWLEDGMENT

This work was supported by the U.S. Department of Energy Office of Inertial Fusion under agreement No. DE-FC08-85DP40200.

PUBLICATIONS AND CONFERENCE PRESENTATIONS

Publications

A. Simon, W. Seka, L. M. Goldman, and R. W. Short, "Raman Scattering in Inhomogeneous Laser-Produced Plasma," *Phys. Fluids* **29**, 1704–1718 (1986).

M. C. Richardson, P. W. McKenty, R. L. Keck, F. J. Marshall, D. M. Roback, C. P. Verdon, R. L. McCrory, J. M. Soures, and S. M. Lane, "High-Aspect-Ratio Laser-Fusion Targets Driven by 24-Beam UV Laser Radiation," *Phys. Rev. Lett.* **56**, 2048–2051 (1986).

R. Q. Gram, H. Kim, J. F. Mason, and M. Wittman, "Ablation Layer Coating of Mechanically Nonsupported Inertial Fusion Targets," *J. Vac. Sci. Technol. A* **4**, 1145–1149 (1986).

H. Kim, S. Noyes, M. C. Richardson, and B. Yaakobi, "Fabrication of Thin Cylindrical Targets for X-Ray Laser Experiments," *J. Vac. Sci. Technol. A* **4**, 1142–1144 (1986).

C. J. McKinstrie and A. Simon, "Nonlinear Saturation of the Absolute Stimulated Raman Scattering Instability in a Finite Collisional Plasma," *Phys. Fluids* **29**, 1959–1970 (1986).

G. Mourou, D. Strickland, and S. Williamson, "How Pulse-Compression Techniques Can Be Applied to High-Energy Laser Amplifiers," *Laser Focus*, 104–106 (June 1986).

B. W. Krakauer, J. S. Gau, and D. J. Smith, "Structural Characterization of Yttrium Oxide Thin Films Using Transmission Electron Microscopy," *J. Mater. Sci. Lett.* **5**, 667–670 (1986).

T. Kessler, W. Seka, J. Kelly, D. Smith, R. Bahr, W. Lockman, N. Wong, and J. Soures, "A Terawatt Nd:Glass Active Mirror System," *High Power and Solid State Lasers* (SPIE, Bellingham, WA, 1986), Vol. 622, pp. 156–160.

Forthcoming Publications

S. D. Jacobs, "Liquid Crystal Devices for Laser Systems," to be published in the *Journal of Fusion Energy*.

R. S. Craxton, R. L. McCrory, and J. M. Soures, "Progress in Laser Fusion," to be published in *Scientific American.*

B. Yaakobi, R. D. Frankel, J. M. Forsyth, and J. M. Soures, "Laser-Generated X-Ray Source for Time-Resolved Biological and Material Structure Studies," to be published in the *Proceedings of a Symposium on New Methods in X-Ray Absorption, Scattering, and Diffraction.*

The following papers are to be published in the *Proceedings of the Workshop on Physics of Laser Fusion,* Vancouver, B.C., June 1985 (*Canadian Journal of Physics*):

A. Simon, "Raman Scattering."

J. Delettrez, "Thermal Electron Transport in Direct-Drive ICF."

L. M. Goldman, W. Seka, K. Tanaka, R. Short, and A. Simon, "The Use of Laser Harmonic Spectroscopy as a Target Diagnostic."

The following articles are to be published in *Physical Review A*:

A. Hauer, R. D. Cowan, B. Yaakobi, O. Barnouin, and R. Epstein, "Absorption-Spectroscopy Diagnosis of Pusher Conditions in Laser-Driven Implosions."

P. A. Jaanimagi, J. Delettrez, M. C. Richardson, and B. L. Henke, "Temporal Dependence of the Mass Ablation Rate in UV-Laser-Irradiated Spherical Targets."

The following papers are to be published in the *Proceedings of the 17th Annual Boulder Damage Symposium*, Boulder, CO, October 1985:

K. A. Cerqua, S. D. Jacobs, B. L. McIntyre, and W. Zhong, "Ion Exchange Strengthening of Nd-Doped Phosphate Laser Glass."

B. Liao, D. J. Smith, and B. L. McIntyre, "The Development of Nodular Defects in Optical Coatings."

D. J. Smith, B. Krakauer, C. J. Hayden, A. W. Schmid, and M. J. Guardalben, "Yttrium-Oxide-Based Anti-Reflection Coating for High Power Lasers at 351 nm."

The following articles are to be published in *Laser Interaction and Related Plasma Phenomena Vol. 7*, edited by G. Miley and H. Hora (Plenum Press, New York, in press):

M. C. Richardson, P. W. McKenty, F. J. Marshall, C. P. Verdon, J. M. Soures, R. L. McCrory, O. Barnouin, R. S. Craxton, J. Delettrez, R. L. Hutchison, P. A. Jaanimagi, R. Keck, T. Kessler, H. Kim, S. A. Letzring, D. M. Roback, W. Seka, S. Skupsky, B. Yaakobi, and S. M. Lane, "Ablatively Driven Targets Imploded with the 24 UV Beam OMEGA System."

M. C. Richardson, G. G. Gregory, R. L. Keck, S. A. Letzring, R. S. Marjoribanks, F. J. Marshall, G. Pien, J. S. Wark, B. Yaakobi, J. D. Goldstone, A. Hauer, G. S. Stradling, F. Ameduri, B. L. Henke, and P. A. Jaanimagi, "Time-Resolved X-Ray Diagnostics for High Density Plasma Physics Studies."

B. Yaakobi, O. Barnouin, C. B. Collins, R. Epstein, A. Hauer, S. A. Letzring, F. J. Marshall, R. L. McCrory, M. C. Richardson, J. M. Soures, and S. Wagel, "Laser-Generated X-Ray Studies Relevant to Compression Diagnostics and Nuclear Level Excitation."

W. C. Mead, S. V. Coggeshall, S. R. Goldman, E. K. Stover, P. D. Goldstone, A. Hauer, V. M. Kindel, L. Montierth, M. C. Richardson, O. Barnouin, P. A. Jaanimagi, R. S. Marjoribanks, R. L. Kauffman, H. Kornblum, and B. F. Lasinski, "Analysis, Modeling, and Design of Short Wavelength Laser Plasma Experiments."

The following articles are to be published in *Review of Scientific Instruments*:

B. Yaakobi, O. Barnouin, M. C. Richardson, J. M. Soures, A. Hauer, and B. Post, "X-Ray Spectroscopic Methods for the Diagnosis of Laser-Imploded Targets."

P. A. Jaanimagi, L. DaSilva, G. G. Gregory, C. Hestdalen, C. D. Kiikka, R. Kotmel, and M. C. Richardson, "Optical Fiducials for X-Ray Streak Cameras at LLE."

P. G. Burkhalter, D. A. Newman, D. L. Rosen, K. Hudson, M. C. Richardson, and P. Audebert, "Spectral Measurement from Laser Produced Plasmas on OMEGA."

S. G. Prussin, S. M. Lane, M. C. Richardson, and S. G. Noyes, "Debris Collection from Implosion of Microballoons."

M. C. Richardson, R. F. Keck, S. A. Letzring, R. L. McCrory, P. W. McKenty, D. M. Roback, J. M. Soures, C. P. Verdon, S. M. Lane, and S. G. Prussin, "Neutron Diagnosis of Compressed ICF Targets."

B. Yaakobi, "X-Ray Diagnostic Methods for Laser-Imploded Targets" and "Thermal Transport, Mass Ablation, and Preheat in Laser-Target Experiments," to be published in the *Proceedings of the Spring College on Radiation in Plasmas*, Trieste, Italy, June 1985 (World Scientific Publishing Co.).

G. Pien, M. C. Richardson, P. D. Goldstone, R. H. Day, F. Ameduri, and G. Eden, "Computerized 3-GHz Multichannel Soft X-Ray Diode Spectrometer for High-Density Plasma Diagnosis," to be published in *Nuclear Instruments and Methods*.

The following articles are to be published in the *Journal of the Optical Society of America B*:

U. Feldman, J. F. Seely, C. M. Brown, J. D. Ekberg, M. C. Richardson, W. E. Behring, and J. Reader, "Spectrum and Energy Levels of Br XXV, Br XXIX, Br XXX, and Br XXXI."

W. E. Behring, C. M. Brown, U. Feldman, J. F. Seely, J. Reader, and M. C. Richardson, "Transitions of the Type 2s-2p in Oxygenlike Y, Zr, and Nb."

P. A. Holstein, J. Delettrez, S. Skupsky, and J. P. Matte, "Modeling Nonlocal Heat Flow in Laser-Produced Plasmas," to be published in the *Journal of Applied Physics*.

J. F. Whitaker, T. Norris, G. A. Mourou, and T. Y. Hsiang, "Pulse Dispersion and Shaping in Microstriplines," to be published in *IEEE Microwave Theory and Techniques Society Transactions*.

M. C. Richardson, B. Yaakobi, R. Epstein, J. Wark, and J. M. Soures, "Imploding Cylindrical Plasmas as X-Ray Laser Media," to be published in the *Proceedings of the 1986 Quebec International Symposium on Optical and Optoelectronic Applied Sciences and Engineering*, Quebec City, June 1986.

Conference Presentations

J. F. Seely, U. Feldman, C. M. Brown, G. Doschek, J. D. Ekberg, W. E. Behring, L. Cohen, M. C. Richardson, and J. Reader, "XUV Spectroscopy of Highly Charged Ions in Line Focus and Point Focus Laser Produced Plasmas," presented at the International Colloquium on X-Ray Lasers, Aussois, France, April 1986.

The following presentations were made at CLEO, San Francisco, CA, June 1986:

T. Kessler, W. Seka, N. Sampat, J. Walker, R. Hutchison, P. Dewa, and S. Swales, "High Power Glass Laser Uniformity: Progress and Prospects."

W. Seka, T. Kessler, G. Brewis, R. Hopkins, J. Kelly, C. D. Kiikka, W. J. Lockman, and S. F. B. Morse, "High Power Glass Laser Front End Design: Coupling of Oscillators to Amplifier Chains."

D. R. Dykaar, G. A. Mourou, M. A. Hollis, B. J. Clifton, K. B. Nichols, C. O. Bozler, and R. A. Murphy, "Picosecond Electro-Optic Characterization of the Permeable Base Transistor."

D. Strickland, P. Maine, M. Bouvier, S. Williamson, and G. Mourou, "Picosecond Pulse Amplification Using Pulse Compression Techniques."

R. L. McCrory, "Direct-Drive Laser Fusion with Submicron Lasers – Prospects for the Late-1980's."

K. A. Cerqua, S. D. Jacobs, K. L. Marshall, A. Lindquist, B. L. McIntyre, and W. Zhong, "Characterization of the Chemical Strengthening of the Nd-Doped Phosphate Laser Glass."

S. D. Jacobs, K. A. Cerqua, K. L. Marshall, T. J. Kessler, R. J. Gingold, P. J. Laverty, and M. Topp, "High Power Laser Beam Apodization Using a Liquid Crystal Soft Aperture."

T. Kessler, W. Seka, J. Kelly, R. Bahr, W. Lockman, and J. M. Soures, "An Active-Mirror-Boosted 351-nm Laser Irradiation Facility."

The following presentations were made at IQEC, San Francisco, CA, June 1986:

M. C. Richardson, P. Audebert, P. A. Jaanimagi, R. L. Keck, F. J. Marshall, R. L. McCrory, P. W. McKenty, D. M. Roback, J. M. Soures, C. P. Verdon, J. S. Wark, and B. Yaakobi, "Ablatively Driven Thick-Shell Target Implosions."

F. J. Marshall, M. C. Richardson, R. L. Keck, P. W. McKenty, D. M. Roback, C. P. Verdon, R. L. McCrory, and J. M. Soures, "High-Neutron-Yield Laser Fusion Target Studies with the 24-Beam UV OMEGA System."

H. Elsayed-Ali, T. Norris, M. Pessot, and G. Mourou, "Femtosecond Time-Resolved Transmissivity of Laser-Heated Thin Copper Films."

S. H. Batha, W. Seka, A. Simon, and L. M. Goldman, "Raman Scattering from Inhomogeneous Plasmas."

W. R. Donaldson, L. Kingsley, G. Mourou, and A. Melissinos, "A Study of the Feasibility of a Laser-Switched Power Linac."

The following presentations were made at the Fifth Topical Meeting on Ultrafast Phenomena, Aspen, CO, June 1986:

D. Strickland, P. Maine, M. Bouvier, S. Williamson, and G. Mourou, "Picosecond Pulse Amplification Using Pulse Compression Techniques."

H. Elsayed-Ali, M. Pessot, T. Norris, and G. Mourou, "Time-Resolved Observation of Electron-Phonon Relaxation During Femtosecond Laser Heating of Copper."

D. R. Dykaar, R. Sobolewski, J. F. Whitaker, T. Y. Hsiang, G. A. Mourou, M. A. Hollis, B. J. Clifton, K. B. Nichols, C. O. Bozler, and R. A. Murphy, "Picosecond Characterization of Ultrafast Phenomena — New Devices and New Techniques."

M. C. Richardson, "High Yield and High Density Ablative Fusion Implosions," presented at the Annual Congress of the Canadian Association of Physicists, Edmonton, Alberta, Canada, June 1986.

K. L. Marshall, S. D. Jacobs, and K. A. Cerqua, "Liquid Crystal Compounds for High-Power Laser Device Applications," presented at the 11th International Liquid Crystal Conference, Berkeley, CA, June/July 1986.

ACKNOWLEDGMENT

The work described in this volume includes current research at the Laboratory for Laser Energetics, which is supported by Empire State Electric Energy Research Corporation, General Electric Company, New York State Energy Research and Development Authority, Ontario Hydro, Southern California Edison Company, the University of Rochester, and the U.S. Department of Energy Office of Inertial Fusion under agreement No. DE-FC08-85DP40200.